Mechanical overstimulation causes acute injury and synapse loss followed by fast recovery in lateral-line neuromasts of larval zebrafish

Melanie Holmgren[1], Michael E. Ravicz[4,5], Kenneth E. Hancock[4,5], Olga Strelkova[4,5], Dorina Kallogjeri[1], Artur A. Indzhykulian[4,5], Mark E. Warchol[1,3], Lavinia Sheets[1,2]*

1. Department of Otolaryngology, Washington University School of Medicine, St. Louis, MO, USA
2. Department of Developmental Biology, Washington University School of Medicine, St. Louis, MO, USA
3. Department of Neuroscience, Washington University School of Medicine, St. Louis, MO, USA
4. Eaton-Peabody Laboratory, Massachusetts Eye and Ear, Boston, Massachusetts, USA
5. Department of Otolaryngology–Head and Neck Surgery, Harvard Medical School, Boston, Massachusetts, USA

*** Corresponding author**

Lavinia Sheets: sheetsl@wustl.edu

Abstract

Excess noise damages sensory hair cells, resulting in loss of synaptic connections with auditory nerves and, in some cases, hair-cell death. The cellular mechanisms underlying mechanically induced hair-cell damage and subsequent repair are not completely understood. Hair cells in neuromasts of larval zebrafish are structurally and functionally comparable to mammalian hair cells but undergo robust regeneration following ototoxic damage. We therefore developed a model for mechanically induced hair-cell damage in this highly tractable system. Free swimming larvae exposed to strong water wave stimulus for 2 hours displayed mechanical injury to neuromasts, including afferent neurite retraction, damaged hair bundles, and reduced mechanotransduction. Synapse loss was observed in apparently intact exposed neuromasts, and this loss was exacerbated by inhibiting glutamate uptake. Mechanical damage also elicited an inflammatory response and macrophage recruitment. Remarkably, neuromast hair-cell morphology and mechanotransduction recovered within hours following exposure, suggesting severely damaged neuromasts undergo repair. Our results indicate functional changes and synapse loss in mechanically damaged lateral-line neuromasts that share key features of damage observed in noise-exposed mammalian ear. Yet, unlike the mammalian ear, mechanical damage to neuromasts is rapidly reversible.

Keywords: Hair cell, mechanical damage, ribbon synapse, inflammation, regeneration

36 Introduction

37 Hair cells are the sensory receptors of the inner ear and lateral-line organs that detect
38 sound, orientation, and motion. They transduce these stimuli through deflection of stereocilia,
39 which opens mechanically-gated cation channels (LeMasurier & Gillespie, 2005; Qiu & Muller,
40 2018) and drives subsequent transmission of sensory information via excitatory glutamatergic
41 synapses (Glowatzki & Fuchs, 2002). Excessive mechanical stimulation, such as loud noise,
42 can damage hair cells and their synaptic connections to afferent nerves. The degree of damage
43 depends on the intensity and duration of the stimulus, with higher levels of traumatic noise
44 producing structural damage to sensory epithelia, including hair cells (Cho et al., 2013;
45 Nordmann, Bohne, & Harding, 2000; Slepecky, 1986) and lower levels leading to various
46 pathologies, including damage to the hair-cell mechanotransduction complex/machinery and
47 stereocilia (Gao, Ding, Zheng, Ruan, & Liu, 1992; Husbands, Steinberg, Kurian, & Saunders,
48 1999), misshapen hair cells (Bullen, Anderson, Bakay, & Forge, 2019), synaptic terminal
49 damage, neurite retraction, and hair-cell synapse loss (Fernandez et al., 2020; Henry & Mulroy,
50 1995; Kujawa & Liberman, 2009; Puel, Ruel, Gervais d'Aldin, & Pujol, 1998). In addition to
51 directly damaging hair cells, excess noise also initiates an inflammatory response (Hirose,
52 Discolo, Keasler, & Ransohoff, 2005; Kaur et al., 2019). Such inflammation is mediated by
53 macrophages, a class of leukocyte that responds to injury by clearing cellular debris and
54 promoting tissue repair (Wynn & Vannella, 2016).

55 The variety of injury and range of severity suggests multiple mechanisms are involved in
56 hair-cell organ damage associated with exposure to strong stimuli. Also unknown are the
57 cellular processes mediating repair following such trauma. While hair cells show a partial
58 capacity for repair of stereocilia and synaptic connections, some sub-lethal damage to hair cells
59 is permanent. Numerous studies of the mammalian cochlea suggest that a subgroup of inner
60 hair-cell synapses are permanently lost following noise exposure (Cho et al., 2013; Hickman,
61 Smalt, Bobrow, Quatieri, & Liberman, 2018; Kujawa & Liberman, 2009; Shi et al., 2013).
62 Glutamate excitotoxicity is likely the pathological event that initiates noise-induced hair-cell
63 synapse loss (Hu, Rutherford, & Green, 2020; Kim et al., 2019; Puel et al., 1998), but the
64 downstream cellular mechanisms are still undefined. Further, the cellular mechanisms that
65 promote hair-cell synapse recovery following damage-induced loss are also not understood.

66 Zebrafish have proven to be a valuable model system for studying the molecular basis of
67 hair-cell injury and repair. Zebrafish sensory hair cells are structurally and functionally
68 homologous to mammalian hair cells (Coffin, Kelley, Manley, & Popper, 2004; Kindt & Sheets,
69 2018; Sebe et al., 2017). In contrast to other vertebrate model organisms, zebrafish hair cells

70 are optically accessible in whole larvae within the lateral-line organs. These sensory organs,
71 called neuromasts, contain clusters of ~ 14 hair cells each and are distributed throughout the
72 external surface of the fish to detect local water movements. Zebrafish can repair and
73 regenerate damaged tissues, including lateral-line organs (Kniss, Jiang, & Piotrowski, 2016;
74 Xiao et al., 2015). This capacity for organ repair combined with optical accessibility allows us to
75 study cellular and synaptic damage and repair *in vivo* following mechanical trauma.
76 In order to model physical damage to hair cell organs in zebrafish lateral line, we
77 developed a protocol to mechanically stimulate the lateral line of free-swimming 7-day-old
78 larvae. Using this protocol, we were able to induce mechanical injury to lateral-line organs that
79 resembled the trauma observed in the mammalian cochlea following acoustic overstimulation.
80 We observed synapse loss in a subset of neuromasts that appeared morphologically intact, as
81 well as hair-cell loss and afferent neurite retraction in a subset of neuromasts that appeared
82 morphologically disrupted. Hair cell mechanotransduction, as measured by uptake of the
83 cationic dye FM1-43, was significantly reduced after mechanical injury. We also observed an
84 inflammatory response similar to that observed in the mammalian cochlea after noise trauma.
85 Remarkably, mechanically induced lateral-line damage appeared to rapidly recover; hair-cell
86 number and morphology returned to normal within 4 hours following exposure, concurrent with
87 clearance of cellular debris by macrophages. Additionally, neuromasts showed partial recovery
88 of afferent innervation within 2 hours following exposure and completely recovered hair-cell
89 morphology and FM1-43 uptake within 4 hours. Cumulatively, these results support that
90 mechanically injured neuromasts show similar features of damage observed in noise exposed
91 ears, yet rapidly repair.

92 Results

93 **Mechanical overstimulation of zebrafish lateral-line hair cells**

94 To mechanically damage hair cells of lateral-line organs in free-swimming 7-day-old
95 zebrafish, we developed a stimulation protocol using an electrodynamic shaker to create a
96 strong water wave stimulus (Fig.1 A). The frequency used for mechanical stimulation was
97 selected and further verified (see Method Details) based on previous studies showing 60 Hz to
98 be within the optimal upper frequency range of mechanical sensitivity of superficial posterior
99 lateral-line neuromasts, which respond maximally between 10-60 Hz, but a suboptimal
100 frequency for hair cells of the anterior macula of the inner ear (Levi, Akanyeti, Ballo, & Liao,
101 2015; Trapani & Nicolson, 2010; Weeg, Fay, & Bass, 2002). Dorsal-ventral displacement of a 6-
102 well dish at 60 Hz and acceleration of 40.3 m/s^2 (+/-0.5m/s^2) created water flow and disturbance
103 of the water surface that was strong enough to trigger 'fast start' escape responses—a behavior

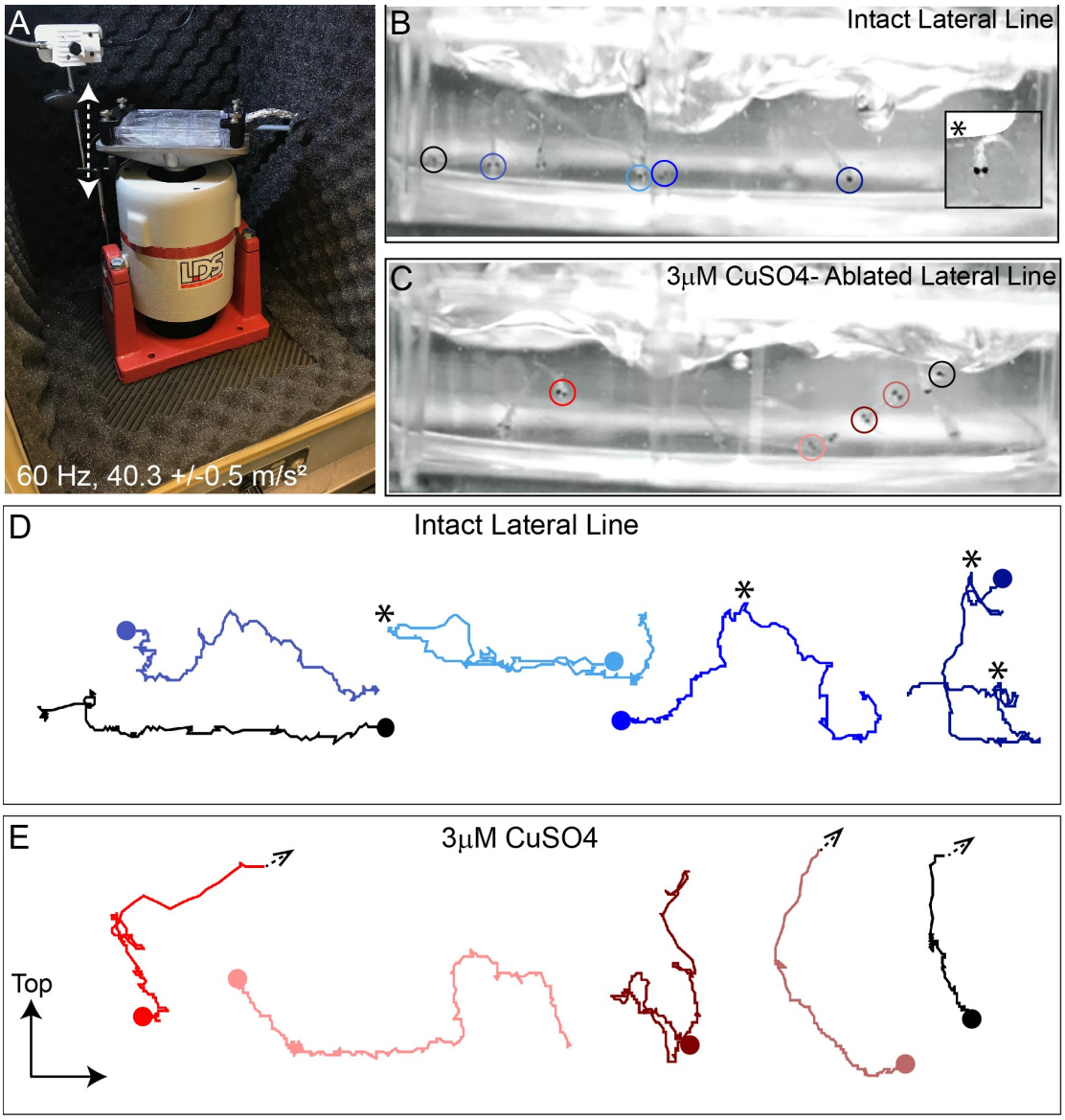

Figure 1: Intense water wave produced by shaker apparatus stimulates lateral-line hair cells and evokes a relevant behavior response. **(A)** The apparatus: a magnesium head expander holding a 6-well dish mounted on a vertically oriented electrodynamic shaker housed inside a sound-attenuation chamber. The stimulus consisted of a 60 Hz vertical displacement of the plate (hatched arrows) driven by an amplifier and controlled by a modified version of the Eaton-Peabody Laboratory Cochlear Function Test Suite. **(B,D)** Swimming behavior of 7-day-old larvae during exposure to the wave stimulus. Traces in (D) represent tracking of corresponding circled fish over 500 ms (1000 fps/ 500 frames). Asterisks indicate a "fast escape" response (B; inset). **(C,E)** Swimming behavior of larvae whose lateral-line neuromasts were ablated with low-dose $CuSO_4$. Arrows in (E) indicate where a larva was swept into the waves and could no longer be tracked.

104 mediated in part by zebrafish lateral-line organs to escape predation (Fig. 1 B inset) (McHenry,
105 Feitl, Strother, & Van Trump, 2009; Nair, Azatian, & McHenry, 2015).
106 'Fast start' escape responses can also be activated by stimulating hair cells of the
107 lateral line and/or the posterior macula in the ear (Bhandiwad, Zeddies, Raible, Rubel, &

108 Sisneros, 2013). To verify that the observed escape responses were mediated predominantly by
109 flow sensed by lateral-line hair cells rather than hair cells of the macula, we exposed a group of
110 larvae to low dose (3μM) copper sulfate ($CuSO_4$) for 1 hour to specifically ablate lateral-line hair
111 cells, but leave hair cells of the ear intact (Olivari, Hernandez, & Allende, 2008). Following a 2
112 hour recovery after $CuSO_4$ treatment, we recorded fish behavior with a high-speed camera
113 during the stimulus (1000 fps for 10 s) and compared the responses of fish with lesioned lateral-
114 line organs with those of untreated control siblings (Fig. 1 B,C; Movie S1,2). When subjected to
115 intense water flow, we found that 'fast start' responses—defined as a c-bend of the body
116 occurring within 15 ms followed by a counter-bend (Burgess & Granato, 2007; McHenry et al.,
117 2009)—occurred significantly less frequently in larvae with ablated lateral line organs than in
118 siblings with intact lateral line (Fig. 1 C,E; avg. 'fast start' responses: : 0.4 (± 0.1)/s in lateral-line
119 ablated vs 1.5 (± 0.1)/s in control; 3 trials,10 s per trial; **P=0.0043). Accordingly, some $CuSO_4$-
120 treated fish were unable to escape the waves and were swept out of view (Fig. 1 E; arrowheads;
121 Movie S2). These observations indicate that the strong water wave generated by our device is
122 stimulating lateral-line hair cells and evoking a behaviorally relevant response.

123 **A subset of mechanically injured neuromasts undergo physical displacement that is**
124 **position dependent but does not require mechanotransduction**

125 To induce mechanical damage to lateral line organs, larvae (10-15 per well) were
126 exposed to an initial 20 minutes of strong water wave stimulus followed by 10 minutes of rest,
127 then 2 hours of continuous stimulus (Supplemental Fig. 1 A). The ten-minute break in exposure
128 was introduced early on when establishing the stimulus duration because it appeared to
129 enhance larval survival; it was therefore maintained throughout the study for consistency. Fish
130 were euthanized and fixed immediately after exposure, then processed for
131 immunohistofluorescent labeling of hair cells and neurons. Unexposed sibling fish served as
132 controls. As posterior lateral-line (pLL) neuromasts have been shown to specifically initiate
133 escape behavior in response to strong stimuli (Liao & Haehnel, 2012), analysis of the
134 morphology of pLL neuromasts L3, L4, and L5 was conducted for exposed and control larvae
135 (Fig. 2 A). Initially, we divided the observed neuromast morphology into two categories:
136 "normal", in which hair cells were radially organized with a relatively uniform shape and size,
137 and "disrupted", in which the hair cells were misshapen and displaced to one side, with the
138 apical ends of the hair cells localized anteriorly (Fig. 2 B, C; see Methods Details for measurable
139 criteria). Position of the neuromast along the tail was also associated with vulnerability to
140 disruption; we observed a gradient of damage in the pLL from rostral to caudal i.e. L5 was more
141

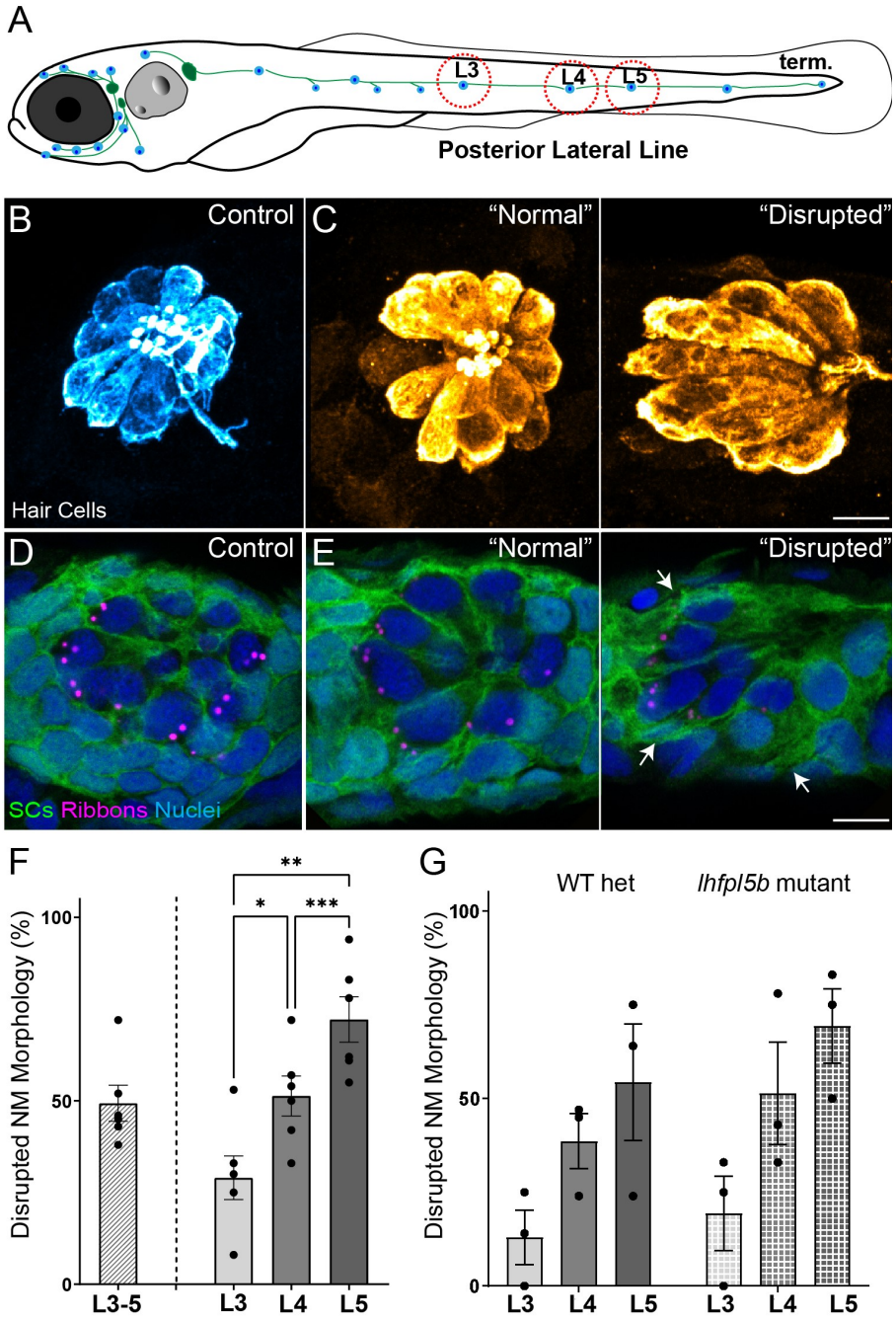

Figure 2: Morphological changes in pLL neuromast hair cells exposed to strong water wave stimulus. **(A)** Schematic of a larval zebrafish. Blue dots indicate neuromasts of the lateral-line organs; green lines indicate innervating afferent lateral-line nerves. pLL neuromasts L3, L4, and L5 were analyzed (dashed circles). **(B-C)** Maximum intensity dorsal top-down 2D projections of confocal images of control or stimulus-exposed neuromast hair cells (blue (B) or orange (C); Parvalbumin immunolabel). Exposed neuromast hair-cell morphology was categorized as "normal" i.e. radial hair-cell organization indistinguishable from control or "disrupted" i.e. asymmetric organization with the hair-cell apical ends oriented posteriorly. **(D)** Maximum intensity projections of supporting cells (SCs) expressing GFP (green), immunolabeled synaptic ribbons (magenta; Ribeye b) and all cell nuclei (blue; DAPI). Note that SCs underlying displaced hair cells also appear physically disrupted (indicated by white arrows). Scale bars: 5 µm **(F)** Average percentage of neuromasts with "disrupted" morphology following mechanical stimulation. Each dot represents the percentage of disrupted neuromasts (NM) in a single experimental trial. Disrupted hair-cell morphology was place dependent, with neuromasts more frequently disrupted following sustained stimulus and when localized toward the posterior end of the tail (*P=0.0386, **P=0.0049, ***P=0.0004) **(G)** Average percentage of exposed neuromasts (NM) with "disrupted" morphology in *lhfpl5b* mutants, which lack mechanotransduction specifically in lateral-line hair cells, vs. heterozygous WT. *lhfpl5b* mutants show a similar gradient of neuromast disruption following mechanical injury as WT siblings. Error Bars = SEM

susceptible to disruption than L4, which was more susceptible to disruption than L3 (Fig. 2 F; Repeated measure One-way ANOVA *P=0.0386, **P=0.0049, ***= 0.0004).

Additionally, we compared mechanical stress from our sustained exposure to an exposure protocol that delivered intermittent pulses of stimulus ("periodic exposure"; Supplemental Fig.1 A). We observed neuromast disruption less frequently with periodic exposures vs. sustained exposure of the same intensity (Supplemental Figure 1 B; Unpaired t-

149 test **P=0.0034), supporting that displacement of neuromasts is a consequence of mechanical
150 injury. Additionally, we examined hair cell morphology in the ears of larvae exposed to sustained
151 stimulus and observed no apparent damage (Supplemental Fig. 2), indicating our
152 overstimulation protocol produces mechanical damage specifically to lateral-line organs.
153 To determine if hair-cell activity plays a key role in the displacement of neuromasts, we
154 exposed *lhfpl5b* mutants—fish that have intact hair cell function in the ear, but no
155 mechanotransduction in hair cells of the lateral line—to sustained stimulation (Erickson,
156 Pacentine, Venuto, Clemens, & Nicolson, 2019). We observed comparable morphological
157 disruption of mutant neuromasts lacking mechanotransduction (Fig. 2 G), suggesting that
158 displacement of lateral-line hair cells is due to physical damage from the stimulus. Further, we
159 observed the adjacent supporting cells in neuromasts with disrupted hair-cell morphology
160 appeared similarly displaced and elongated (Fig. 2 E "disrupted"; white arrows), indicating that
161 mechanical injury disrupts the structural integrity of the entire neuromast organ.

162 **Hair-cell loss and reduced afferent innervation correspond to neuromast disruption**

163 Moderate noise exposures can cause damage or loss of cochlear hair-cell synapses,
164 including swelling and retraction of afferent nerve fibers, while more extended and/or severe
165 exposures lead to hair-cell loss. To address whether mechanical damage in the lateral line
166 produced similar morphological changes, we surveyed the number of hair cells per neuromast
167 and the percentage of neuromast hair cells lacking afferent innervation in fish immediately
168 following exposure to sustained stimulation (Fig. 3). We observed a reduction in the number of
169 hair cells per neuromast immediately following exposure (Fig. 3 D, E; **Adj P=0.0019; N=13
170 trials) as well as a significant reduction in the percentage of hair cells per neuromast innervated
171 by afferent neurons (Fig. 3 F, G; ****Adj P<0.0001; N=12 trials).
172 As described in Fig. 2 F, we found on average ~half of L3-L5 neuromasts examined
173 showed "disrupted" hair-cell morphology immediately following sustained stimulus exposure. To
174 define the associations between overall neuromast morphology and specific structural changes
175 in mechanically injured neuromasts, we examined the numbers of hair cells and the percent of
176 hair cells contacted by afferent fibers in exposed neuromasts parsed into "normal" and
177 "disrupted" morphologies. With hair cell number, we observed significant loss specifically in
178 "disrupted" neuromasts, while "normal" neuromast hair-cell number appeared comparable to
179 control (Fig. 3 D, E; Adj P=0.3859 normal, ****Adj P<0.0001 disrupted). With hair-cell afferent
180 innervation we observed a similar trend i.e., a significant number of hair cells lacked afferent
181 innervation in stimulus exposed neuromasts with "disrupted" morphology, but not "normal"
182 neuromasts (Fig. 3 F,G; Adj P=0.7503 normal, ****Adj P<0.0001 disrupted).

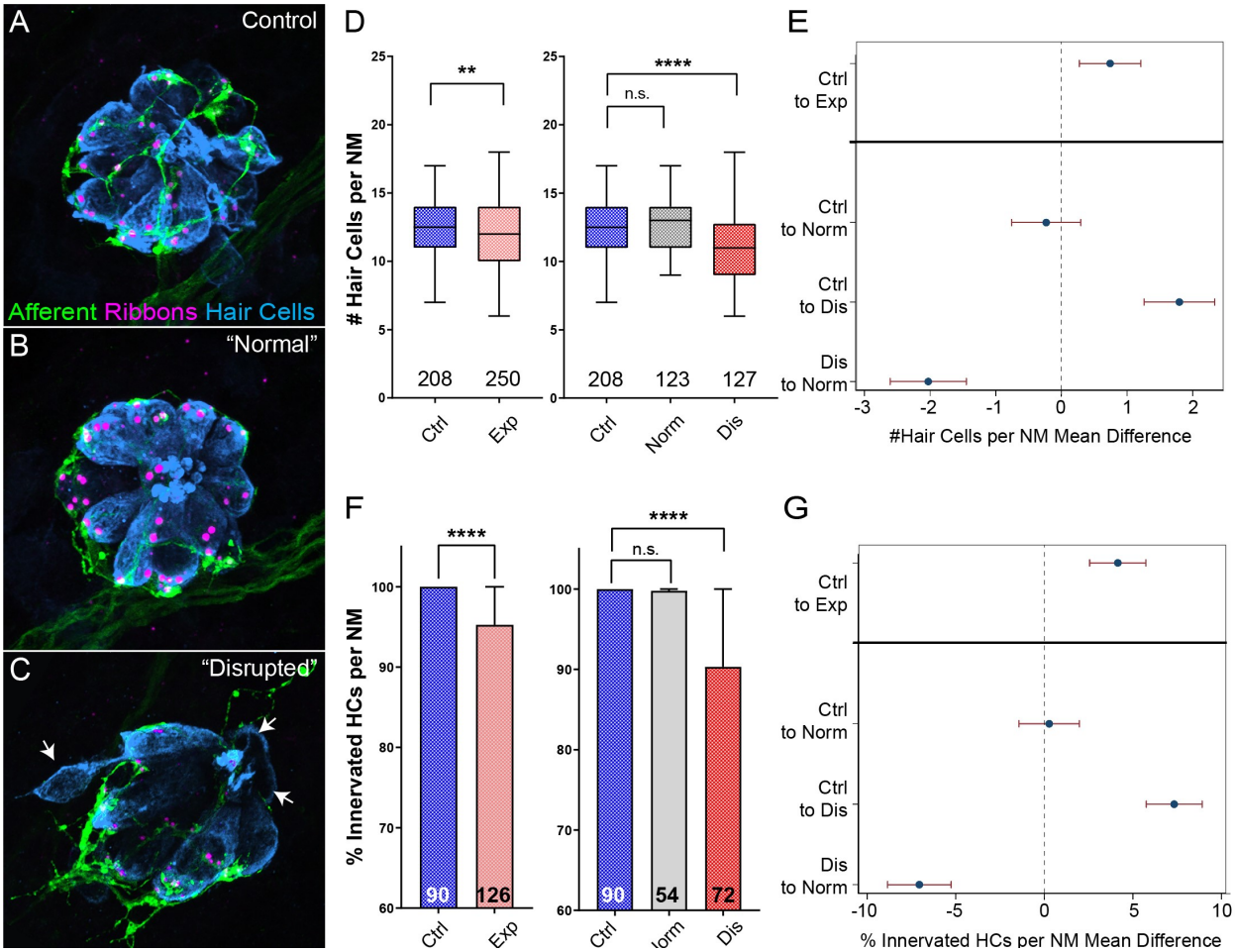

Figure 3: Hair-cell loss and de-innervation is specific to "disrupted" neuromasts.
(A-C) Representative maximum intensity projection images of control (A) or exposed lateral line neuromasts with "normal" (B) or "disrupted" (C) morphology immediately following sustained strong wave exposure (0h). Synaptic ribbons (magenta; Ribeye b) and hair cells (blue; Parvalbumin) were immunolabled. Afferent neurons were expressing GFP. Scale bar: 5 µm **(D)** Hair-cell number per neuromast immediately post exposure. A significant reduction in hair cell number was observed (**Adj P=0.0019) and was specific to "disrupted" neuromasts (Adj P=0.3859 normal, ****Adj P<0.0001 disrupted). Pink box plot (Exp) represents pooled exposed neuromasts, while gray (Norm) and red (Dis) plots represent neuromasts parsed into normal and disrupted groups. Numbers beneath each plot indicate the number of neuromasts per group. Whiskers = min to max **(E)** Differences of least squares means in hair cell number per neuromast between groups. Bars represent 95% confidence interval (CI). **(F)** Percentage of neuromast hair cells innervated by afferent nerves. Numbers within each bar indicate the number of neuromasts per group. A significant portion of neuromast hair cells lacked afferent innervation following exposure (****Adj P<0.0001). Hair cells lacking afferent innervation were specifically observed in disrupted neuromasts (Adj P=0.7503 normal, ****Adj P<0.0001 disrupted). **(G)** Differences of least squares means in % hair cells innervated per neuromast between groups. Bars represent 95% CI

Mechanically overstimulated neuromasts with "normal" morphology lose a greater number of hair-cell synapses when glutamate clearance is inhibited

Hair cells contain electron-dense presynaptic specializations—called dense bodies or synaptic ribbons—apposing afferent PSDs which constitute afferent synaptic contacts (Davies, Tingley, Kachar, Wenthold, & Petralia, 2001; Sheets, Trapani, Mo, Obholzer, & Nicolson, 2011).

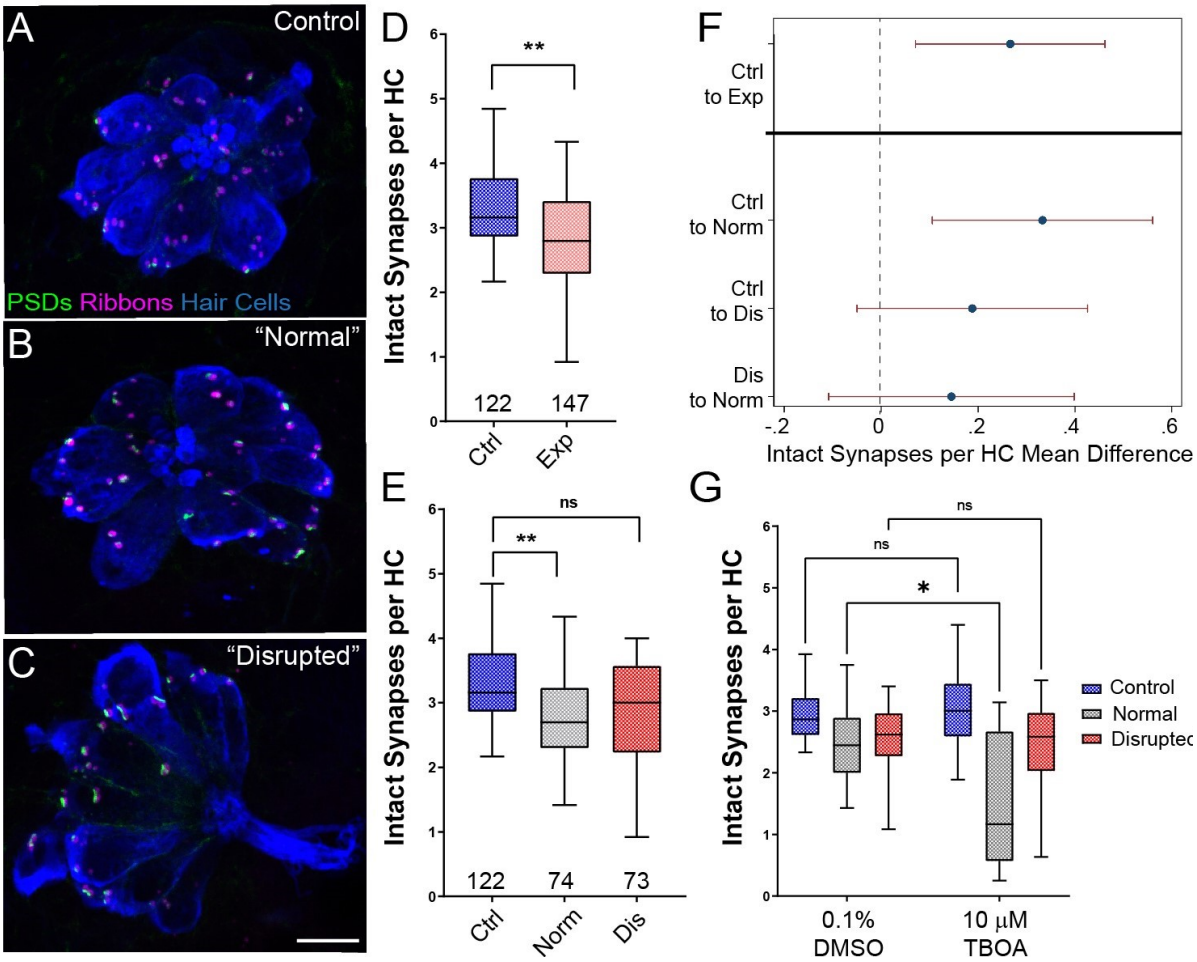

Figure 4: Significant hair-cell synapse loss is observed in "normal" neuromasts following mechanical overstimulation and exacerbated by blocking glutamate uptake. **A-C)** Representative maximum intensity projection images of unexposed (A), or stimulus exposed lateral-line neuromast with "normal" (B) or "disrupted" (C) morphology. Synaptic ribbons (magenta; Ribeye b), PSDs (green; MAGUK) and hair cells (blue; Parvalbumin) were immunolabled. Scale bar: 5 µm **(D-E)** Intact synapses per neuromast hair cell. Pink box plot in D (Exp) represents pooled exposed neuromasts while, in E, gray (Norm) and red (Dis) plots represent neuromasts parsed into normal and disrupted groups. Whiskers =min to max. The average number of intact synapses per hair cell was significantly reduced in exposed neuromasts (D; **Adj P=0.0078); when parsed, this reduction was significant in the "normal" exposure group relative to control (E; **Adj P=0.0043 normal, Adj P=0.1207 disrupted). **(F)** Differences of least squares means in number of intact synapses per hair cell between groups. Bars represent 95% CI. **(G)** The number of intact synapses per hair cell in larvae co-treated with TBOA, to block glutamate clearance, or drug carrier alone during exposure. Synapse loss was significantly greater in "normal" neuromasts co-exposed to TBOA compared to fish co-exposed to the drug carrier alone (Two-way ANOVA. *P<0.0187).

188 In the larval zebrafish lateral line, afferent nerve fibers innervate multiple hair cells per
189 neuromast forming ~3-4 synaptic contacts per hair cell. To determine whether strong water
190 wave stimulus exposure generated lateral-line hair-cell synapse loss, we counted the number of
191 intact synapses (ribbons juxtaposed to PSDs; Fig. 4 A-C) in control and exposed larvae. We
192 observed significant reduction in the number of intact synapses per hair cell following sustained

exposure (Fig. 4 D, F; **Adj P=0.0078). When we compared “normal” and “disrupted” neuromasts following exposure, we observed a loss of intact synapses per hair cell in all exposed neuromasts, with significantly fewer synapses in “normal” exposed neuromasts relative to control (Fig. 4 E-F; **Adj P=0.0043 normal, Adj P=0.1207 disrupted). Additionally, significant synapse loss was observed in the neuromasts of fish exposed to the less mechanically damaging “periodic” stimulus (Supplemental Fig. 1 F’).

Previous studies indicate that excess glutamate signaling may be a key factor driving inner hair-cell synapse loss following exposure to damaging noise (Chen, Kujawa, & Sewell, 2010; Kim et al., 2019). We therefore inhibited glutamate clearance from neuromast hair-cell synapses by pharmacologically blocking uptake with the glutamate transporter antagonist Threo-beta-benzyloxyaspartate (TBOA) during sustained stimulus exposure. We observed a significantly greater degree of hair-cell synapse loss in stimulated neuromasts with “normal” morphology co-treated with TBOA than in stimulated neuromasts co-treated with drug carrier alone (Fig. 4 E; Two-way ANOVA. *P<0.0187), suggesting glutamate excitotoxicity contributes to hair-cell synapse loss observed in mechanically overstimulated neuromasts with intact morphology.

To further characterize synapse loss in relation to afferent neurite retraction, we examined fish in which we immunolabeled synaptic ribbons, PSDs, afferent nerve fibers, and

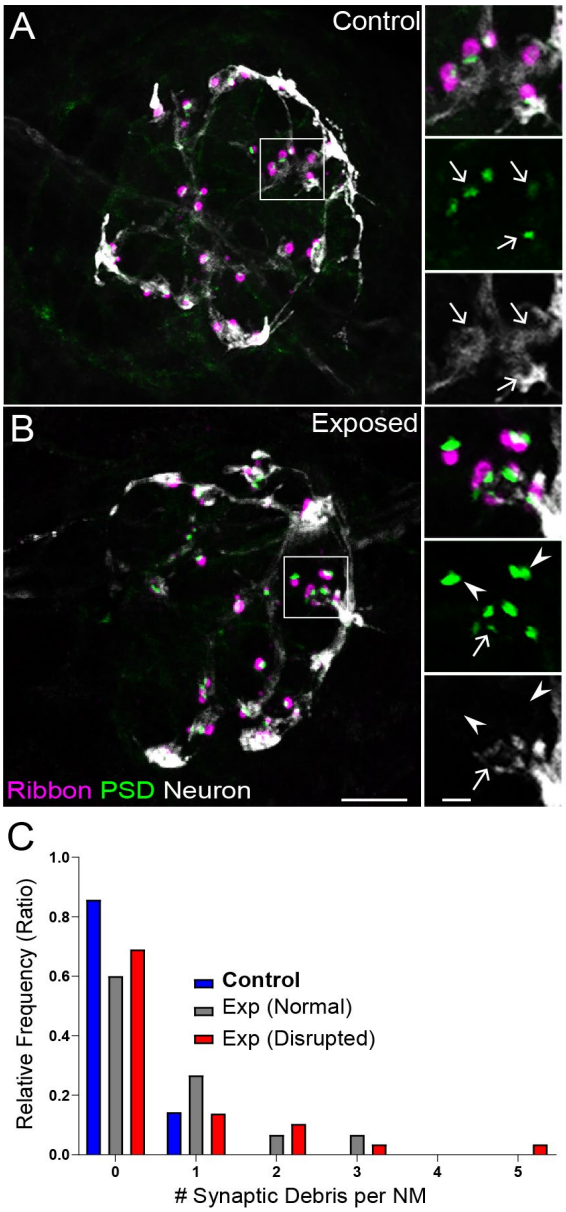

Figure 5: Mechanically overstimulated neuromasts showed retracted neurites and detached synaptic debris. **(A-B)** Representative images of control (A) and exposed (B) neuromasts. Synaptic ribbons (magenta; Ribeye b) and PSDs (green; MAGUK) were immunolabeled; hair cells were also immunolabeled, but not shown for clarity. Afferent neurons (white) were labeled with GFP. Insets: Arrows indicate intact synapses adjacent to afferent neurons; arrowheads (B) indicate synaptic debris. Scale bars: 5µm (main panels), 1µm (insets). **(C)** Frequency histogram of observed synaptic debris per neuromast (NM). While control neuromasts occasionally had 1 detached synapse, exposed neuromasts were observed that had up to 5 detached synapses.

227 hair cells (Fig. 5 A,B). We then quantified instances where synapses, i.e. juxtaposed pre- and
228 postsynaptic components associated with hair cells, were no longer adjacent to an afferent
229 nerve terminal. As these synapses appeared detached and suspended from their associated
230 neurons, making them no longer functional, we refer to them as synaptic debris. While we rarely
231 observed synaptic debris in unexposed neuromasts, we observed a greater relative frequency
232 of synaptic debris in neuromasts exposed to strong water wave stimulus (Fig. 5 C; One sample
233 Wilcoxon test, P=0.1250 (control), *P=0.0313(normal), **P=0.0039(disrupted)). Taken together,
234 we observed two distinct types of morphological damage to afferent synapses in mechanically
235 overstimulated neuromasts: loss of synapses within neuromasts that appear intact that is
236 exacerbated when glutamate uptake is blocked and a higher incidence of synaptic debris that
237 appear detached from afferent neurites in all exposed neuromasts.

238 **Mechanically overstimulated lateral line neuromasts show signs of hair-cell injury and**
239 **macrophage recruitment**

240 The inner ears of birds and mammals possess resident populations of macrophages,
241 and additional macrophages are recruited after acoustic trauma or ototoxic injury (Warchol,
242 2019). A similar macrophage response occurs at lateral line neuromasts of larval zebrafish after
243 neomycin ototoxicity (Warchol, Schrader, & Sheets, 2021). Analysis of fixed specimens, as well
244 as time-lapse imaging of living fish (e.g., Hirose, Rutherford and Warchol, 2017), has
245 demonstrated that macrophages migrate into neomycin-injured neuromasts and actively
246 phagocytose the debris of dying hair cells. To determine whether a similar inflammatory
247 response also occurs after mechanical injury to the lateral line, we characterized macrophage
248 behavior after sustained stimulation. These studies employed Tg(*mpeg1:yfp*) transgenic fish,
249 which express YFP in all macrophages and microglia. Fish were fixed immediately after
250 exposure, or allowed to recover for 2, 4 or 8 hours. Control fish consisted of siblings that
251 received identical treatment but were not exposed to mechanical stimulation. Data were
252 obtained from the two terminal neuromasts from the pLL of each fish (Fig. 6 A). In agreement
253 with data shown in Fig. 3 D, we observed a modest but significant decline in hair-cell number in
254 specimens that were examined immediately and at 2 hours after sustained exposure (Fig. 6 B;
255 **P<0.003). Consistent with earlier studies (Hirose, Rutherford, & Warchol, 2017), 1-2
256 macrophages were typically present within a 25 μm radius of each neuromast (Fig. 6 C). In
257 uninjured (control) fish, those macrophages remained outside the sensory region of the
258 neuromast and rarely contacted hair cells. However, at 2, 4 and 8 hours after sustained
259 stimulus, we observed increased macrophage-hair cell contacts (Fig. 6 D; *P=0.024), as well as
260 the presence of immunolabeled hair-cell debris within macrophage cytoplasm (suggestive of

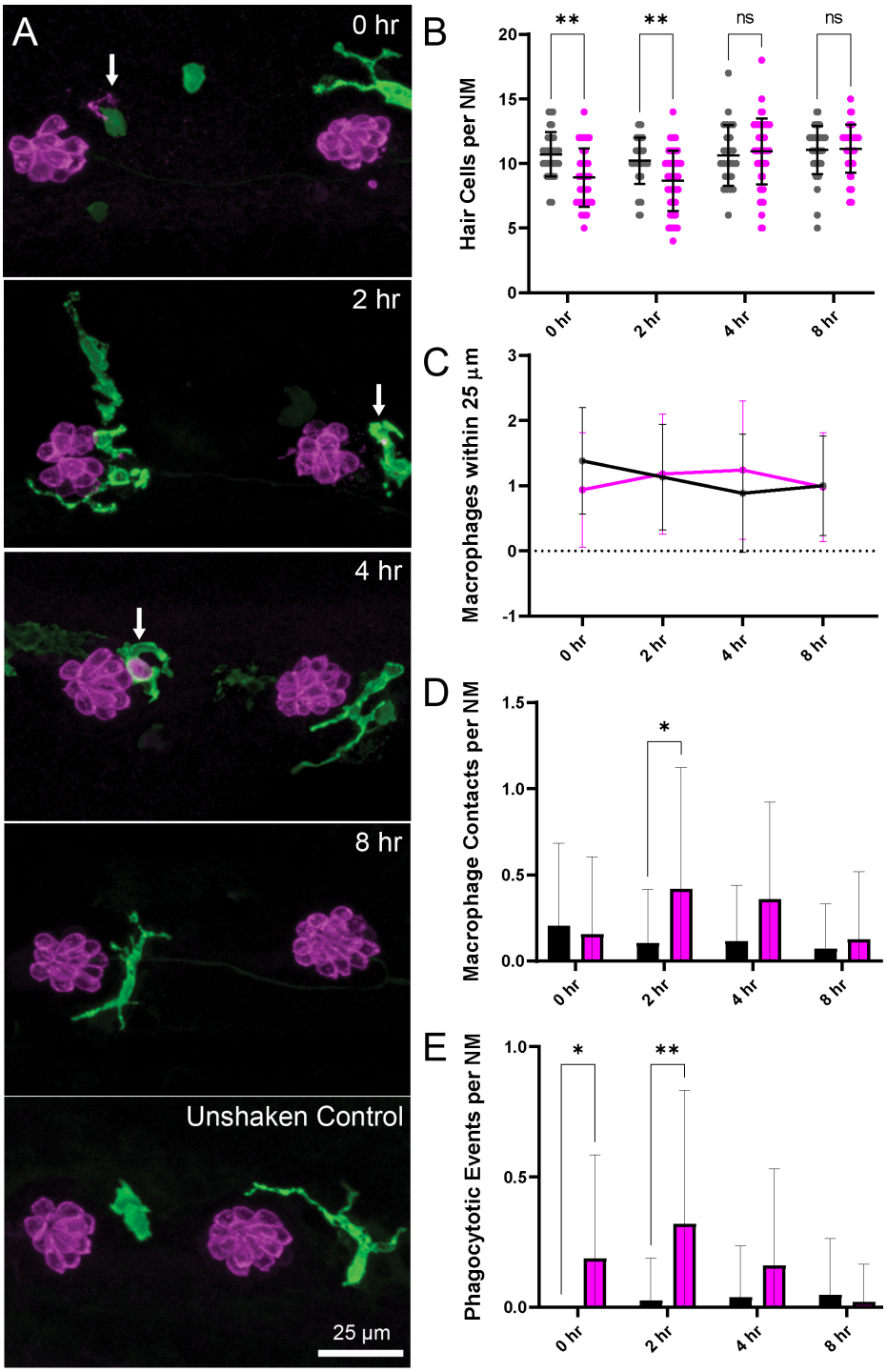

Figure 6. Macrophage response to mechanical overstimulation of lateral line hair cells. Experiments used fish that express YFP under regulation of the macrophage-specific *mpeg1* promoter. All images and data were collected from the two distal-most neuromasts of the posterior lateral line (Fig 2A; term). **(A)** Macrophages (green) responded to mechanical injury by entering neuromasts, contacting hair cells and internalizing otoferlin-labeled debris (arrows, magenta). Images show examples of macrophage behavior at different time points after noise trauma. **(B)** Quantification of hair cell number, which was significantly reduced at 0-2 hr after noise exposure (Mixed-effects analysis: **P<0.003). **(C)** Quantification of macrophages within a 25 µm radius of the terminal neuromasts at 0-8 hr after noise injury. Most neuromasts possessed 1-2 nearby macrophages and this number was not changed by noise exposure. **(D)** Quantification of direct contacts between macrophages and hair cells. Macrophage-hair cell contacts were counted at each survival time after noise exposure and normalized to the total number of sampled neuromasts. Increased levels of contact were observed at 2 and 4 hr after noise (*P=0.0243). **(E)** Quantification of phagocytosis as a function of post-noise survival time. Macrophages that had internalized otoferlin-labeled material were counted at each time point and normalized to the total number of sampled neuromasts. The percentage of macrophages that contained such debris was significantly increased at 0-2 hr after strong water wave stimulus (*P=0.0465; **P=0.0013). Data were obtained from 26-50 neuromasts/time point. Error Bars = SD

phagocytosis, Fig. 6 A, 4 h., arrow). Macrophage-hair cell contact and phagocytosis peaked at 2 hours after exposure (Fig. 6 E; **P= 0.0013 (2 h)). Notably, the numbers of macrophages within a 25 µm radius of each neuromast remained unchanged at all time points after exposure, suggesting that the inflammatory response was mediated by local macrophages and that mechanical injury did not recruit macrophages from distant locations (Fig. 6 C). This pattern of

injury-evoked macrophage behavior is qualitatively similar to the macrophage response observed in the mouse cochlea after acoustic trauma (Hirose et al., 2005; Kaur et al., 2019; Kaur et al., 2015).

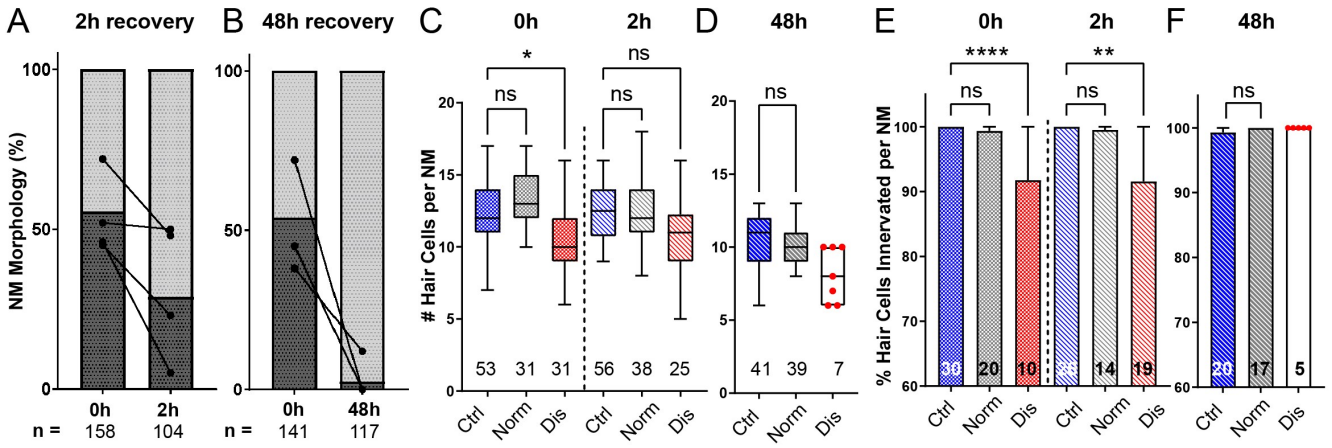

Figure 7: Mechanically overstimulated neuromasts recover hair-cell morphology, hair-cell number, and innervation. **(A,B)** Average percentage of exposed neuromasts with "normal" vs. "disrupted" morphology following exposure. Each dot represents the percentage of disrupted neuromasts (L3-L5) in a single experimental trial; lines connect data points from the same cohort of exposed fish following 2 hours (A) or 48 hours (B) recovery. **(C,D)** Multilevel analysis of hair-cell number per neuromast immediately (0 h) post-exposure or after 2 or 48 hour recovery. Numbers beneath each plot indicate the number of neuromasts per group. Whiskers =min to max. Morphologically "disrupted" neuromasts has significantly fewer hair cells at 0h but not 2h following exposure (C; *Adj P=0.0321 (0h disrupted), Adj P=0.1875 (2h disrupted). Most exposed neuromasts were morphologically "normal" following 48h recovery and had a comparable number of hair cells relative to control (D; Adj P=0.4443). **(E,F)** The percentage of "disrupted" neuromast hair cells lacking afferent innervation was significant following 0h and 2h recovery (E; ****Adj P<0.0001 (0h disrupted), **Adj P=0.0016 (2h disrupted)). All hair cells were fully innervated following 48h recovery, including the few neuromasts with "disrupted" morphology (F; aligned red dots).

Mechanically injured neuromasts rapidly repair following exposure

To determine if damage to mechanically injured neuromasts was progressive, persistent, or reversible, we compared neuromast morphology, hair-cell number, and innervation at 0 hours, 2 hours, and 48 hours following sustained exposure to strong water wave stimulus. We observed a decrease in the percentage of neuromasts showing "disrupted" morphology 2 hours following exposure, relative to fish fixed immediately following exposure (Fig. 7 A; 54% disrupted (0 h) vs. 32% disrupted (2 h); N=4 trials), suggesting that physical disruption of neuromast morphology following mechanical injury is rapidly reversible. Consistent with this observation, the average hair-cell number per neuromast at 2 hours post-exposure appeared to recover (Fig. 7 C; *Adj P=0.0321 (0h disrupted), Adj P=0.1875 (2h disrupted); N=6 trials). Recovery of hair-cell number occurred within 2-4 hours (Fig. 6 A, B) and corresponded with macrophages infiltrating neuromasts and phagocytosing hair-cell debris (Fig. 6 A, E). We also observed, compared to immediately following exposure, a lesser degree of afferent fiber

retraction (Fig. 7 E; ****Adj P<0.0001 (0h disrupted), **Adj P=0.0016 (2h disrupted); N=6 trials) indicating partial recovery of innervation.

A recent study characterized zebrafish lateral-line hair-cell damage induced by exposure to ultrasonic waves and reported a delayed hair-cell death and synapse loss 48-72 hours following exposure (Uribe et al., 2018). To determine if lateral line neuromasts exposed to the strong wave stimulus generated by our apparatus underwent delayed hair-cell loss, we examined hair-cell morphology, number, and innervation 48 hours following sustained stimulus exposure. Most exposed neuromasts examined showed “normal” HC morphology (Fig. 7 B) with no significant difference in hair-cell number (Fig. 7 D; Adj P=0.4443; N=4 trials). Hair-cell afferent innervation after 48 hours was comparable to control fish; even the few neuromasts that remained morphologically “disrupted” were fully innervated (Fig. 7 F).

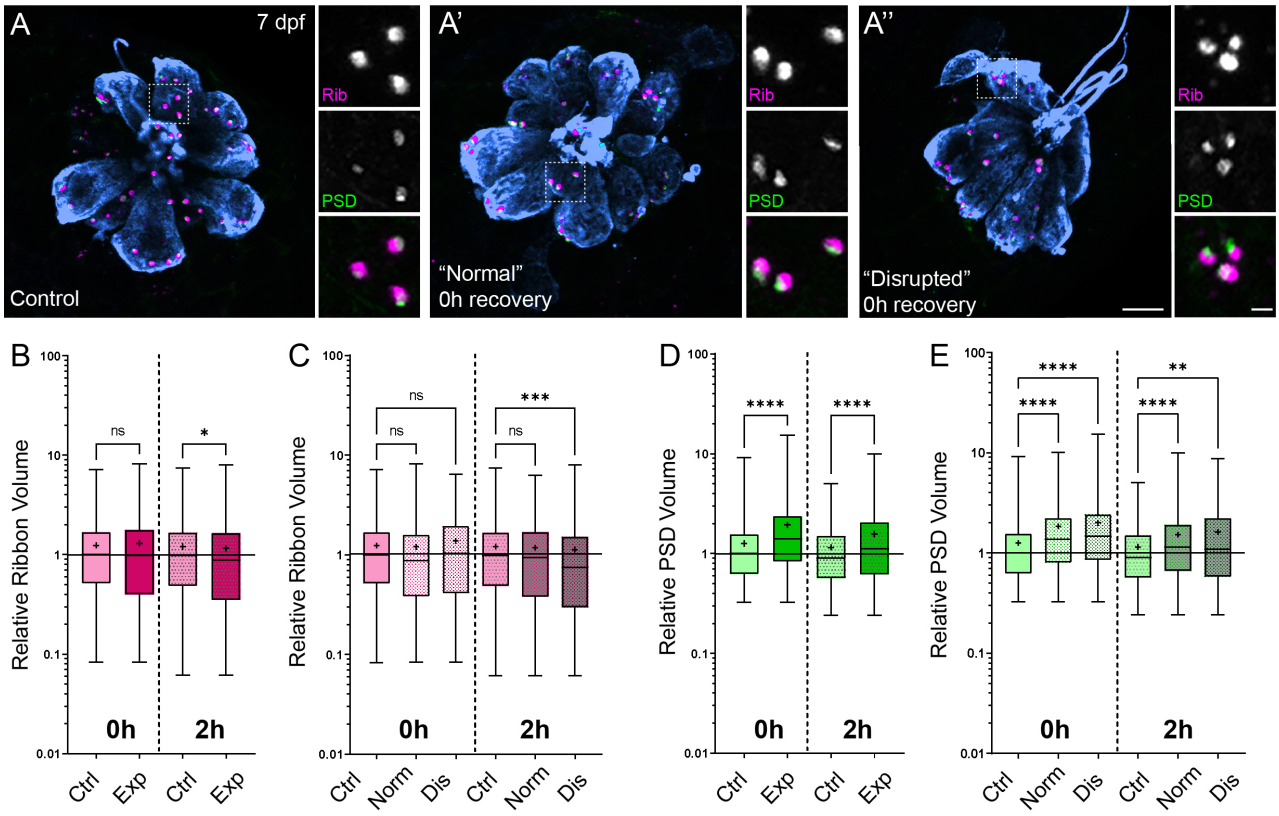

Figure 8: Changes in synaptic ribbon and PSD sizes following sustained mechanical overstimulation. **(A-A’’)** Representative images of control (A) and exposed (A’, A”) neuromasts. Synaptic ribbons (magenta; Ribeye b), PSDs (green; MAGUK), and hair cells (blue, Parvalbumin) were immunolabeled. Scale bars: 5µm (main panels), 1µm (insets). **(B-E)** Box and whisker plots of relative synapse volumes normalized to 0h control. Whiskers indicate the min. and max. values; “+” indicates the mean value, horizontal lines indicate the relative median value of the control. (B) Ribbon volume appeared comparable to control immediately following exposure but was reduced 2 hours after exposure (*P=0.0195). (C) Significant reduction in ribbon size relative to control was specific to disrupted neuromasts (Kruskal-Wallis test: ***P=0.0004 (2h)). (D) Significantly larger PSDs were observed both immediately and 2 hours following exposure (****P<0.0001). (E) Enlarged PSDs were present in both “normal” and “disrupted” exposed neuromasts, with a greater enlargement observed 0h post-exposure (Kruskal-Wallis test: ****P<0.0001 (0h) ; ***P=0.0001, **P=0.0024 (2h)).

293 **PSDs are enlarged in all neuromasts following mechanical overstimulation**

294 Previous studies in mice and guinea pigs indicate moderate noise exposures modulate
295 the size of synaptic components (Kim et al., 2019; Song et al., 2016). To determine if pre- and
296 postsynaptic components were also affected in our model, we compared the relative volumes of
297 neuromast hair-cell presynaptic ribbons and their corresponding PSDs in control and stimulus
298 exposed larvae. We observed a moderate reduction in synaptic-ribbon size following exposure;
299 ribbon volumes were significantly reduced relative to controls following 2 hours recovery (Fig. 8
300 B; Kruskal-Wallis test *P=0.0195; N=3 trials), and this reduction was specific to “disrupted”
301 neuromasts (Fig. 8 C). While the changes in ribbon volume we observed were modest and
302 delayed in onset, we saw dramatic enlargement of PSDs immediately and 2 hours following
303 exposure (Fig. 8 D; Kruskal-Wallis test ****P<0.0001; N=3 trials). In contrast to the observed
304 reduction in ribbon size, relative PSD volumes were significantly enlarged in all exposed
305 neuromasts regardless of whether neuromast morphology was “normal” or “disrupted” (Fig. 8
306 E). These data reveal enlarged PSDs as the predominant structural change in mechanically
307 overstimulated neuromast hair-cell synapses.

308 **Mechanically injured neuromasts have damaged kinocilia, disrupted hair-bundle**
309 **morphology, and reduced FM1-43 uptake immediately following exposure**

310 An additional consequence of excess noise exposure in the cochlea is damage to
311 mechanosensitive hair bundles at the apical end of hair cells and, correspondingly, disruption of
312 mechanotransduction (Wagner & Shin, 2019). Larval zebrafish lateral-line hair cells each have a
313 hair bundle consisting of a single kinocilium flanked by multiple rows of actin-rich stereocilia
314 (Kindt, Finch, & Nicolson, 2012). To determine if our exposure protocol damaged apical hair-cell
315 structures, we used confocal imaging and scanning electron microscopy (SEM) to assess hair
316 bundle morphology in both unexposed control larvae and larvae fixed immediately following
317 sustained exposure. All neuromasts throughout the fish were evaluated, but to remain
318 consistent with our fluorescence imaging results, we closely assessed the appearance of the
319 caudal pLL neuromasts. We found the caudal neuromasts to be more damaged than the ones
320 positioned more rostrally: the frequency of neuromasts with apparently disrupted appearance
321 increased the closer its position to the tail (Supplemental Fig. 3). This is consistent with our
322 fluorescence observations (Fig. 2 F; Supplemental Fig. 4 B) in which L5 neuromasts were more
323 likely to be disrupted than more anteriorly positioned L3.

324 A closer examination of neuromast morphology revealed a difference of the kinocilia
325 length and bundling. The neuromasts of the control fish carry a bundle of long (10-15 μm),
326 uniformly shaped kinocilia (Fig. 9 A-E). In contrast, the neuromasts of the fish fixed immediately

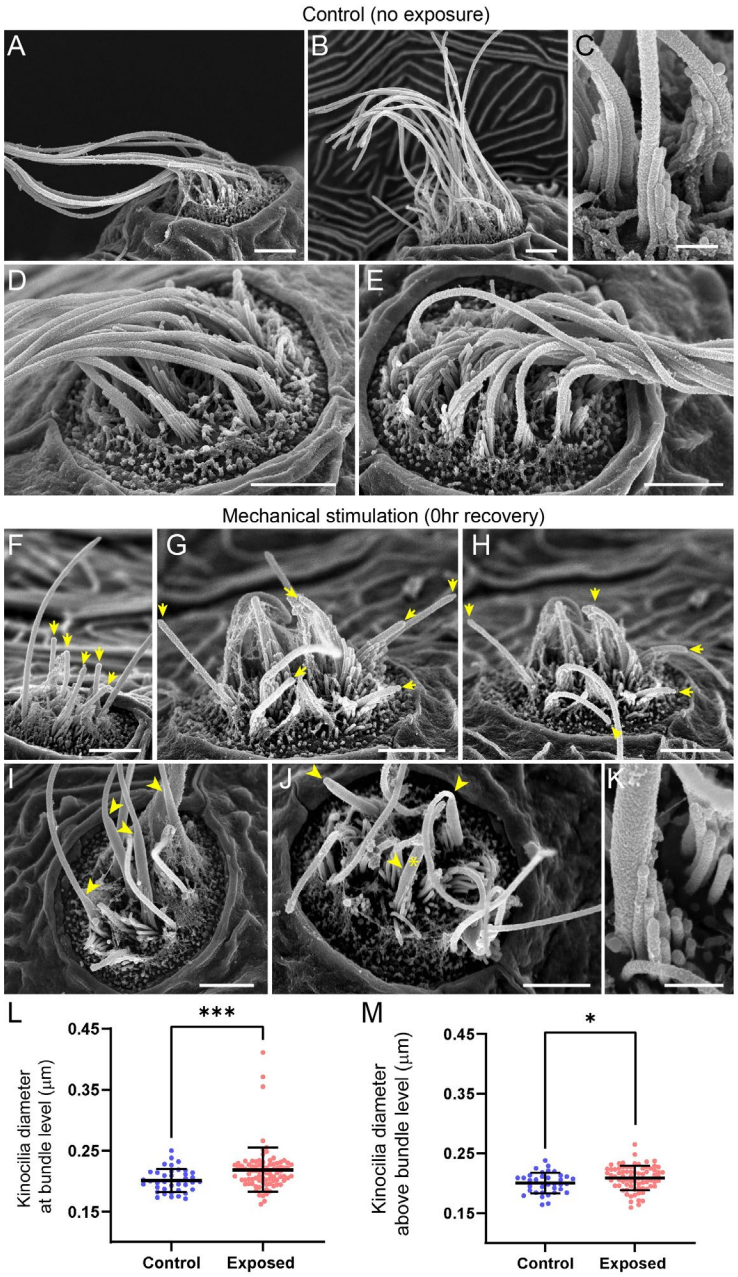

***Figure 9: Scanning electron microscopy imaging of neuromasts following mechanical injury reveals disorganized hair cell stereocilia bundles and damaged kinocilia*. (A-E)** Representative images of tail neuromasts of control fish larvae. Each hair cell carries a kinocilium, which is visibly thicker than its neighboring actin-filled, mechanosensitive stereocilia: see panel C featuring both structures at higher magnification (the kinocilium diameter is 220 nm, while stereocilia measured 90-110 nm). The kinocilia of control neuromasts are long (10-15 µm) and bundled together, while the stereocilia bundles have an apparent staircase arrangement. **(F-K)** Representative images of damaged tail neuromasts immediately following noise exposure featuring short (F-H, yellow arrows), disorganized (G, H), and swollen (I-K, yellow arrowheads) kinocilia, and disorganized stereocilia. (K) Same stereocilia bundle as in J marked with an asterisk at higher magnification to highlight the difference in the diameter of the kinocilium (360 nm) and neighboring stereocilia (85-100 nm) for noise exposed hair cells, as compared to the control hair cells in C. Scale bars: A, B, D-J – 2 µm; C, K – 500 nm. **(L-M)** Kinocilia diameter at bundle level (L; Mann Whitney test ***P=0.0007) and 3-5 µm above bundle level (M; Welch's t test *P=0.0243). Exposed NM data in L were not normally distributed (D'Agostino-Pearson test ****P<0.0001). Error Bars = SD

after sustained exposure often appear to carry much shorter kinocilia (Fig. 9 F-H, yellow arrows), which lack bundling and, in some cases, pointing to different directions (Fig. 9 G,H). The apparent kinocilia length difference between control and overstimulated neuromasts suggests at least some kinocilia may undergo a catastrophic damage event at the time of stimulation, as their distal parts break off the hair cells. This is further supported by some

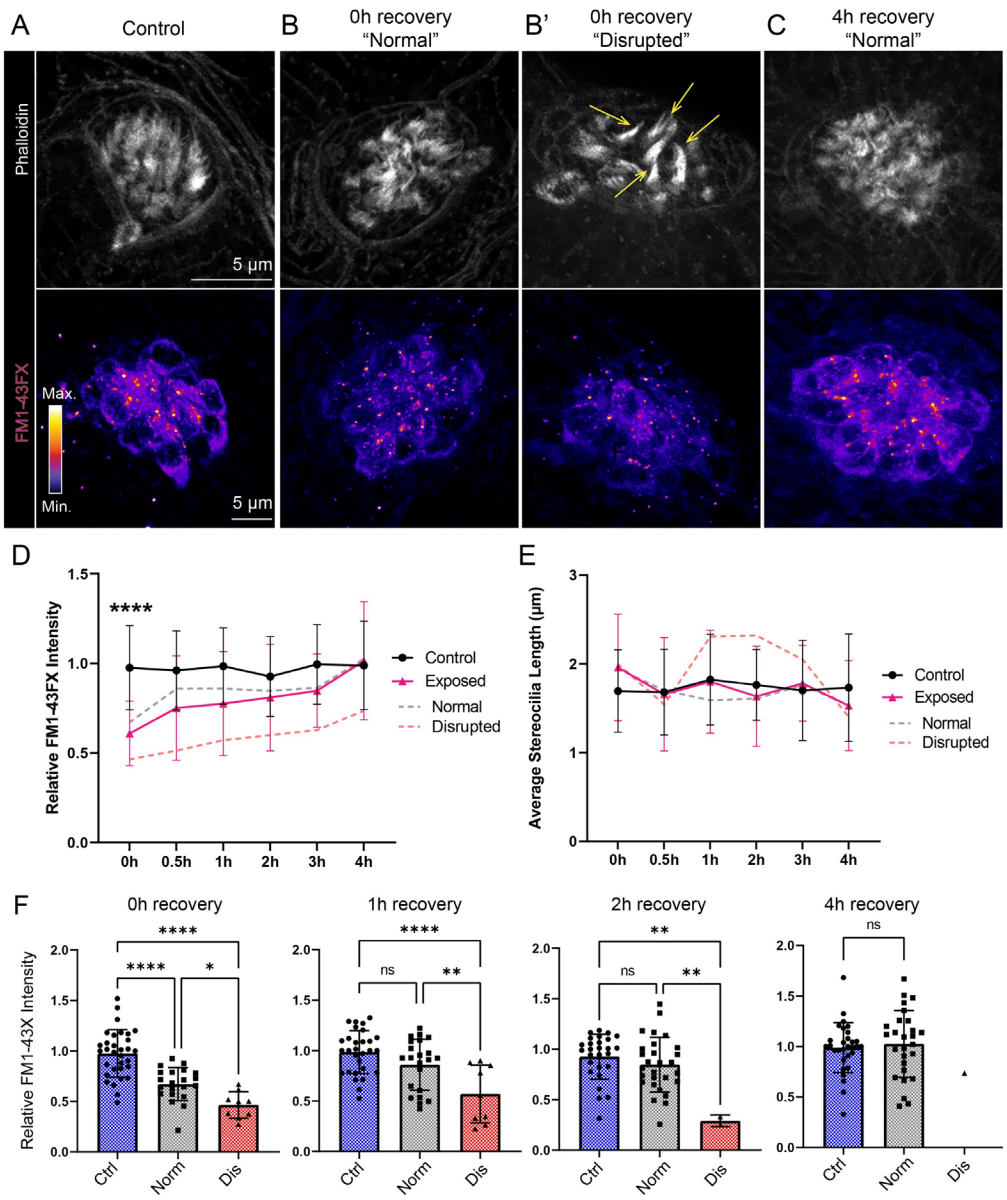

Figure 10: Hair cell mechanotransduction was significantly reduced but rapidly recovered following mechanical overstimulation. **(A-C)** Representative images of hair-cell stereocilia (conjugated phalloidin, gray) and FM1-43FX fluorescence intensity of the corresponding neuromast in representative control (A) or mechanically overstimulated fish immediately (B, B') or 4 hours (C) following exposure. Yellow arrows in (B') indicate phalloidin labeling that appeared tapered. **(D)** Average relative FM1-43FX fluorescence intensity measurements in control and exposed neuromasts over 4 hours of recovery. FM1-43FX uptake was significantly reduced in exposed neuromasts immediately following mechanical overstimulation but appear to completely recover by 4 hours (Tukey's multiple comparisons test ****P<0.0001 (0h), P=0.0579 (1h), P=0.8387 (2h), P=0.8387 (4h)). Dashed lines indicate FM1-43FX fluorescence intensity measurements in exposed neuromasts parsed into "normal" and "disrupted" morphologies. **(E)** Average stereocilia length of centrally localized hair bundles in control and exposed neuromasts. Dashed lines indicate measurements in exposed neuromasts parsed into "normal" and "disrupted" morphologies. Error Bars = SD **(F)** Relative FM1-43FX fluorescence in both "normal" and "disrupted" exposed neuromasts was significantly reduced immediately following exposure but recovered over time (Tukey's multiple comparisons test ****P<0.0001, *P=0.0328 (0h); ****P<0.0001, **P=0.0098 (1h); **P=0.0025 control vs. dis, **P=0.0089 normal vs. dis (2h)). Each point represents an individual neuromast. Nearly all observed exposed neuromasts appeared morphologically normal following 4 hours; note only one neuromast data point in the disrupted category of the 4h recovery graph. Data were obtained from 26-32 neuromasts per condition over three trials.

examples of kinocilia with thicker, 'swollen' proximal shafts closer to the cuticular plate of the cell, some of which extend into a thinner distal part while others appear to lack the distal part

completely (Fig. 9 I-K, yellow arrowheads). Accordingly, the average diameter of kinocilia at the level of the hair bundle (L2-5) was significantly larger than control, with a few kinocilia showing dramatically thicker widths ~2x greater than the thickest control (Fig. 9 L; ***P=0.0007). When measured ~3-5 µm above the bundle, the exposed neuromast kinocilia have a somewhat larger average diameter relative to control, but not as dramatic as observed at the base (Fig. 9 M; *P=0.0243). Stereocilia bundles from both groups of animals carried tip links, but we were unable to systematically evaluate and quantify their abundance. However, we observed signs of damaged bundle morphology following overstimulation, as they often appeared splayed, with gaps between the rows of stereocilia (Fig. 9 I-K).

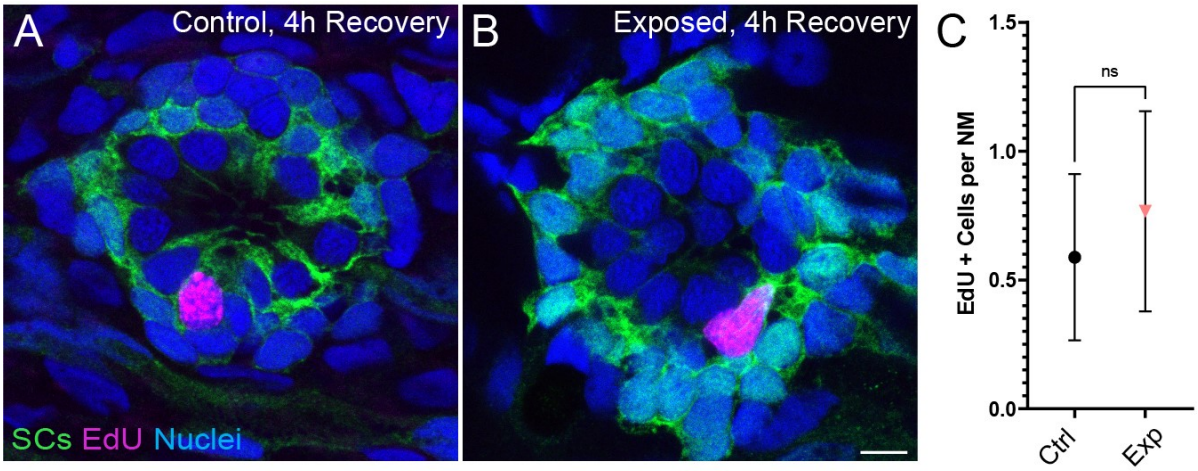

Figure 11: Neuromasts show no change in cell proliferation following mechanical overstimulation. **(A,B)** Representative cross-section images of EdU (magenta) labeling of proliferating neuromast cells. Fish were exposed to EdU for 4 hours following stimulus exposure. Supporting cells (SC) were expressing GFP. Scale bars: 5µm **(C)** Average number of EdU+ cells per neuromast were comparable in control and exposed larvae. Data were obtained from 33-34 neuromasts per condition over three trials. (Two-way ANOVA. P=0.4193) Bars represent 95% CI.

To evaluate the effect of mechanical overstimulation on hair bundle function in relation to hair bundle morphology, we assessed mechanotransduction by briefly exposing free-swimming larvae to the fixable mechanotransduction-channel permeable dye FM1-43X (Holmgren & Sheets, 2021; Toro et al., 2015). We treated control and mechanically overstimulated larvae with FM1-43X immediately and at several time points up to 4 hours following exposure, then fixed the larvae and co-labeled hair-cell stereocilia with fluorescently-conjugated phalloidin (Fig. 10 A-C). We observed a significant reduction in the relative intensity of FM1-43 in all exposed neuromasts immediately following exposure (Fig. 10 D, F (0h); ****P<0.0001). While phalloidin labeling of stereocilia revealed what appeared to be tapered hair bundles in some exposed neuromasts (Fig. 10 B'; yellow arrows), average stereocilia length obtained from 3D interpolated confocal image stacks was not significantly altered (Fig. 10 E). Remarkably, FM1-43FX uptake

354 showed recovery within 30 minutes and fully recovered over several hours. (Fig. 10 C, D). The
355 degree of FM1-43FX fluorescence recovery following mechanical damage appeared to
356 correspond with recovery of neuromast morphology; following 4 hours, nearly all neuromasts
357 exposed to strong wave stimulus showed “normal” morphology and relative FM1-43X
358 fluorescence that was comparable to control (Fig 10 D, F, 4h recovery). This observed timeline
359 of morphological recovery coincides with macrophage recruitment and phagocytosis hair cell
360 debris peaking 2 hours post exposure (Fig 6 D,E) followed by full recovery of hair cell number
361 between 2-4 hours post exposure (Fig 6 B). Additionally, we quantified proliferating neuromast
362 cells by treating control and mechanically overstimulated 5-ethynyl-2-deoxyuridine (EdU) larvae
363 for 4 hours following exposure and saw no difference in the number of EdU positive cells per
364 neuromast in each condition (Fig 11 A-C). Cumulatively, these data support that most damaged
365 hair cells are repaired within mechanically injured neuromasts.

366 Discussion

367 To model mechanical injury resulting from noise trauma in the zebrafish lateral line, we
368 describe here a method to mechanically overstimulate neuromasts of the posterior lateral line.
369 Using this method, we observed: i) hair-cell synapse loss in a subset of stimulus exposed
370 neuromasts with intact morphology, ii) morphological displacement, hair-cell loss, and afferent
371 deinnervation in a subset of mechanically disrupted neuromasts, iii) an inflammatory response
372 that peaked 2-4 hours following stimulus exposure, iv) kinocilia and hair bundle damage, and v)
373 reduced FM1-43 uptake in all immediately following exposure. Remarkably, mechanically
374 injured neuromasts rapidly recover following exposure; neuromast morphology, innervation, and
375 mechanotransduction showed significant recovery within an hour, and most neuromasts were
376 completely recovered within 4 hours post exposure.

377 **Zebrafish lateral-line as a model for sub-lethal mechanical damage and noise-induced**
378 **synapse loss**

379 Mechanical damage to the zebrafish lateral line induced by strong water wave stimulus
380 is observable immediately following exposure, is specific to the lateral-line organ, and appears
381 to be rapidly repaired. These observations contrast with a recently published noise damage
382 protocol for larval zebrafish which used ultrasonic transducers (40-kHz) to generate small,
383 localized shock waves (Uribe et al., 2018). They reported delayed hair-cell death and modest
384 synapse loss that was not apparent until 48 hours following exposure, was not accompanied by
385 decreased mechanotransduction, and was observed in the inner ear as well as the lateral-line
386 organs. Some of the features of the damage they observed—delayed onset apoptosis and hair-
387 cell death—may correspond to lethal damage following blast injuries. We propose features of

388 the damage we observe with our stimulus protocol—reduced mechanotransduction, hair-cell
389 synapse loss, and rapid inflammatory response—may correspond to sub-lethal noise-induced
390 damage of hair-cell organs. Because of differences in the nature of the stimuli in these two
391 studies, it is difficult to directly compare the pathological outcomes. Mechanical overstimulation
392 in the Uribe et al., study was induced using ultrasonic (40 kHz) actuators. Such high frequencies
393 are far outside those that are detected by lateral line neuromasts (Levi et al., 2015; Trapani &
394 Nicolson, 2010) supporting that cavitation in the water medium is likely causing the observed
395 damage. In contrast, our study delivered a stimulus of high intensity 60 Hz water waves directly
396 to the fish. This frequency is within the range of sensitivity of lateral line neuromasts of larval
397 zebrafish and evoked a lateral-line mediated behavior (Fig 1 B, C) suggesting that the hair cells
398 were being directly stimulated by the water motion. The present method more closely resembles
399 the techniques that are typically used to study noise damage in the mammalian cochlea, where
400 high intensity acoustic energy causes hair cell and synaptic injury in specific regions of the
401 cochlea that are best-responsive to the frequency of the stimulus. This idea is further supported
402 by the observation that synapse loss in hair cells exposed to strong wave stimulation is greater
403 when glutamate uptake is blocked (Fig. 4 E), suggesting a shared mechanism of glutamate
404 excitotoxicity between noise-exposed mammalian ears and strong water wave stimulus exposed
405 lateral-line organs (Kim et al., 2019; Sebe et al., 2017).

406 **Disruption of neuromast morphology is a consequence of mechanical injury**

407 Strong water wave exposure produced a percentage of pLL neuromasts that were
408 morphologically “disrupted”. Several observations support that such “disrupted” neuromasts
409 represent mechanical injury to neuromast organs. One is that *lhfpl5b* mutant neuromasts, which
410 lack mechanotransduction specifically in lateral-line hair cells, were comparably vulnerable to
411 physical disruption as their wild-type siblings (Fig. 2 G; (Erickson et al., 2019)). This finding
412 supports that hair-cell activity during stimulation does not underly the physical displacement of
413 hair cells observed following strong water wave stimulus. Additionally, physical disruption of the
414 neuromast affects the whole organ—hair cells and their adjacent supporting cells (Fig. 2 D).
415 This observation contrasts with what is observed in mammalian ears exposed to high intensity
416 noise, where mechanical injury to outer hair cells is localized to stereocilia disruption (H. Wang,
417 Yin, Yu, Huang, & Wang, 2011). Speculatively, displacement of hair cells in mechanically
418 injured neuromasts may be due to loss of structural support from displaced supporting cells. As
419 the lateral-line organs are superficially localized on the surface of the skin, some of the intense
420 mechanical tension applied across the tail is likely coupled to neuromasts leading to the
421 physical displacement of a subset of exposed neuromasts. Finally, we observed reduced FM1-

422 43 uptake in “disrupted” neuromasts (Fig. 10 G) and measurable changes kinocilia likely
423 reflecting mechanical damage (Fig. 9; (Wagner & Shin, 2019)). It is notable how rapidly
424 mechanically disrupted lateral-line neuromasts regain normal morphology and FM1-43 uptake
425 (Fig. 10). The superficial lateral line’s direct exposure to the environment may require more
426 robust mechanisms for repair, unlike hair cell organs of mammals which are encased in bone.

427 **Hair-cell overstimulation and synapse loss**

428 In contrast to de-innervation and modest hair-cell loss we observed in mechanically
429 disrupted neuromasts, we saw significant loss of hair-cell synapses in neuromasts that were
430 exposed to strong water wave stimulus but not mechanically disrupted i.e. “normal” (Fig. 4). Two
431 notable observations were made in exposed neuromasts regarding synapse loss. First, loss of
432 synapses in “normal” exposed neuromasts was markedly more severe when synaptic glutamate
433 clearance was inhibited (Fig. 4 G), suggesting that synapse loss may reflect moderate hair-cell
434 damage resulting from overstimulation of hair cells and excess glutamate accumulation.
435 Involvement of glutamate signaling as a key mediator of noise-induced synapse loss has
436 recently been reported in mice; loss of glutamate signaling prevents noise-induced synapse loss
437 and pharmacologically blocking postsynaptic Ca^{2+} permeable AMPA receptors protects against
438 cochlear hair-cell synapse loss from moderate noise exposure (Hu et al., 2020; Kim et al.,
439 2019). Second, synapse loss occurred in neuromasts that appeared to be fully innervated (Fig.
440 3 B, Fig. 4 B). This observation was initially surprising given that pharmacologically activating
441 evolutionarily conserved Ca^{2+} permeable AMPARs has been shown to drive afferent terminal
442 retraction in the zebrafish lateral line (Sebe et al., 2017). We propose that subtle damage to
443 afferents in “normal” exposed neuromasts may accompany synapse loss but not be apparent as
444 loss of innervation, as single afferent processes innervate multiple hair cells of the same polarity
445 within an individual neuromast (Dow, Jacobo, Hossain, Siletti, & Hudspeth, 2018; Faucherre,
446 Pujol-Marti, Kawakami, & Lopez-Schier, 2009). This idea is further supported by our observation
447 that the relative frequency of synaptic debris (i.e. synaptic components that appear detached
448 from afferent neurites) was higher in exposed neuromasts with “normal” morphology relative to
449 control (Fig. 5 C). We speculate that synaptic debris observed in exposed neuromasts with
450 “normal” morphology may be the result of excitotoxic damage at synaptic terminals (Sebe et al.,
451 2017) while synaptic debris observed in “disrupted” neuromasts may reflect mechanical
452 disruption of supporting cells and retraction of afferent innervation from a subset of hair cells
453 (Fig 3 C, F).

454 In addition, glutamate signaling may not be the only driver of synapse loss resulting from
455 excess stimulation. Studies in zebrafish and mice support that mitochondrial stress combined

456 with excessive synaptic activity may also contribute to hair-cell synapse loss (X. Wang et al.,
457 2018; Wong et al., 2019). Future work using this model to examine the effect of excess
458 mechanical stimulation on mutants with reduced glutamate release or impaired glutamate
459 clearance (to elevate or reduce glutamate in the synaptic cleft, respectively) combined with
460 modified mitochondrial function may define the relative roles of glutamate excitotoxicity and hair-
461 cell mitochondrial stress to synaptic loss.

462 **Role of inflammation following mechanical injury to lateral-line organs**

463 Our results indicate that mechanical injury to neuromasts evokes an inflammatory
464 response. Prior studies of larval zebrafish have shown that macrophages reside near the
465 borders of uninjured neuromasts and migrate into neuromasts after ototoxic injury (Hirose et al.,
466 2017). We found that macrophages migrate into neuromasts within ~2 hours of mechanical
467 injury, where they contact hair cells and, in some cases, engulf hair-cell debris. Although this
468 macrophage response is similar to that which occurs after ototoxic injury to neuromasts (Carrillo
469 et al., 2016; Hirose et al., 2017; Warchol et al., 2021), the extent of hair cell loss after
470 mechanical overstimulation is much less than the injury that occurs after ototoxicity. We
471 observed macrophage entry in 30-40% of exposed neuromasts, despite modest hair cell loss
472 (Fig. 6 B,D). It is possible that the morphological changes characteristic of mechanically injured
473 neuromasts are accompanied by the release of macrophage chemoattractants. In addition,
474 studies of noise exposure to the mammalian cochlea indicate that high levels of synaptic activity
475 (without accompanying hair cell loss) can evoke macrophage migration to the synaptic region
476 (Kaur et al., 2019). In either case, the signals responsible for such recruitment remain to be
477 identified. The observation that macrophages had internalized immunolabeled hair-cell material
478 further suggests that recruited macrophages engage in the phagocytosis of hair cell debris, but
479 it is not clear whether macrophages remove entire hair cells or target specific regions of cellular
480 injury (e.g., synaptic debris; Fig. 5). In any case, our data indicate that the macrophage
481 response to mechanical injury of zebrafish lateral-line neurons is similar to that which occurs
482 after noise injury to the mammalian cochlea (Warchol, 2019) and suggests that zebrafish may
483 be an advantageous model system in which to identify the signals that recruit macrophages to
484 sites of excitotoxic injury.

485 **Hair-cell synapse morphology following mechanical overstimulation**

486 Immediately following mechanical overstimulation, the most pronounced morphological
487 change we observed in hair-cell synapses was significantly enlarged PSDs (Fig. 8 D, E).
488 Speculatively, PSD enlargement may be a consequence of reduced glutamate release from hair

489 cells following sustained intense stimulation. Mice and zebrafish fish lacking hair-cell
490 glutamatergic transmission have enlarged postsynaptic structures (Kim et al., 2019; Sheets,
491 Kindt, & Nicolson, 2012), indicating that glutamate may regulate postsynaptic size. While our
492 data do not directly support this idea, we speculate that reduced glutamatergic transmission in
493 mechanically overstimulated neuromasts may be a consequence of transiently impaired
494 mechanotransduction (Fig. 10 B,D; (Zhang et al., 2018)). Alternatively, cholinergic efferent
495 feedback, which has been shown to hyperpolarize lateral-line hair cells, may reduce hair-cell
496 excitability during sustained strong wave exposure to protect against excess glutamate release,
497 excitotoxic damage, and synapse loss (Carpaneto Freixas et al., 2021). Interestingly,
498 presynaptic ribbons were not similarly enlarged, but instead showed a modest reduction in size
499 following mechanical injury. Functional imaging of zebrafish lateral line has shown that a subset
500 of hair cells in each neuromast are synaptically silent, and these silent hair cells can become
501 active following damage (Zhang et al., 2018). As ribbon size has been observed to correspond
502 with synaptic activity (Merchan-Perez & Liberman, 1996; Sheets et al., 2012), reduction in
503 ribbon size may reflect recruitment of synaptically silent hair cells following mechanically-
504 induced damage. Future functional studies are needed to determine if mechanical
505 overstimulation recruits more active hair-cell synapses, and to verify whether glutamate release
506 from active synapses is reduced following mechanical overstimulation.

507 **Lateral-line neuromasts fully recover following mechanical damage**

508 Previous studies indicate mammalian cochlear hair cells have some capacity for repair
509 following sub-lethal mechanical damage, including tip-link repair and regeneration of a subset of
510 ribbons synapses (Indzhykulian et al., 2013; Jia, Yang, Guo, & He, 2009; Kim et al., 2019). But
511 such ability is limited, and our understanding of hair-cell repair mechanisms is incomplete. By
512 contrast, we observe complete recovery of neuromast morphology and innvervation following
513 mechanical trauma to the zebrafish lateral line. The cellular mechanisms responsible for such
514 repair are not fully defined, but may involve regulation of neurite growth, glutamate signaling,
515 inflammation, and/or neurotrophic factors (Kaur et al., 2019; Kim et al., 2019; Wan, Gomez-
516 Casati, Gigliello, Liberman, & Corfas, 2014). Further study using this zebrafish model of
517 mechanical overstimulation may provide insights that will assist in the development of methods
518 for promoting complete hair-cell repair following damaging stimuli to the mammalian cochlea.

519 We also found that mechanical trauma resulted in a small degree of hair-cell loss in
520 disrupted neuromasts (Fig. 3D), but that hair-cell numbers had recovered after 2 hours (Fig.
521 6B). The mechanism that mediates this recovery is not clear, but it is notable that a low level of
522 hair cell production normally occurs in lateral line neuromasts of larval zebrafish, as part of a

523 process of ongoing turnover (Cruz et al., 2015; Williams & Holder, 2000). In the present study,
524 we observed a small amount of proliferation in neuromasts of both mechanically-damaged and
525 control fish. Since mechanical damage did not increase the level of cell proliferation in
526 neuromasts relative to control (Fig 11), we believe this observed cell division is likely associated
527 with the turnover process. Hair-cell regeneration in the vertebrate inner ear can also occur via
528 direct phenotypic conversion of supporting cells into a replacement hair cells (Warchol, 2011).
529 While it is conceivable that transdifferentiation of supporting cells could occur within 2 hours of
530 mechanical injury, such transdifferentiation has not been previously demonstrated in zebrafish
531 lateral line neuromasts (e.g. (Thomas et al., 2015)). Overall, these observations indicate that
532 mechanical trauma does not increase the rate of hair-cell production within neuromasts, further
533 supporting that neuromast recovery is largely due to hair-cell repair.
534 In summary, our data show that exposure of zebrafish lateral-line organs to strong water
535 wave results in mechanical injury and loss of afferent synapses, but that these injuries rapidly
536 recover. Our next steps will be to define the time course for synaptic recovery and to determine
537 how lateral-line mediated behavior is affected by mechanically induced damage. Sub-lethal
538 overstimulation of hair cells in the zebrafish lateral line provides a useful model for defining
539 mechanisms of damage and inflammation and for identifying pathways that promote hair-cell
540 repair following mechanically-induced injury.
541
542 Declaration of interests:
543 The authors declare no competing financial or non-financial interests.
544
545 Acknowledgments: This work was supported by the National Institute on Deafness and Other
546 Communication Disorders R01DC016066 (L.S.), R01DC017166 (A.A.I), and R01DC006283
547 (M.E.W.), Washington University Dept. of Otolaryngology (L.S.), and the Amelia Peabody
548 Charitable Fund (L.S.). We would like to thank Valentin Militchin (WashU) and Evan Foss (Mass
549 Eye and Ear) for engineering support and Mark Rutherford for thoughtful feedback on the
550 manuscript.
551

552 Method Details

553 ***Ethics Statement***

554 This study was performed with the approval of the Institutional Animal Care and Use
555 Committee of Washington University School of Medicine in St. Louis and in accordance with
556 NIH guidelines for use of zebrafish.

557 ***Zebrafish***

558 All zebrafish experiments and procedures were performed in accordance with the
559 Washington University Institutional Animal Use and Care Committee. Adult zebrafish were
560 raised under standard conditions at 27-29°C in the Washington University Zebrafish Facility.
561 Embryos were raised in incubators at 29°C in E3 media (5 mM NaCl, 0.17 mM KCl, 0.33 mM
562 $CaCl_2$, 0.33 mM $MgCl_2$; (Nüsslein-Volhard & Dahm, 2002)) with a 14 h:10 h light:dark cycle. After
563 4 dpf, larvae were raised in 100-200 ml E3 media in 250-ml plastic beakers and fed rotifers
564 daily. Sex of the animal was not considered in our studies because sex cannot be predicted or
565 determined in larval zebrafish.

566 The transgenic lines *TgBAC(neurod1:EGFP)* (Obholzer et al., 2008),
567 *Tg(tnks1bp1:EGFP)* (Behra et al., 2012), *Tg(-6myo6b:βactin-EGFP)* (Kindt et al., 2012) and
568 *Tg(mpeg1:YFP)* (Roca & Ramakrishnan, 2013) were used in this study. Fluorescent larvae were
569 identified at 3 dpf without anesthesia in E3 media. The mutant line *lhfpl5b*$^{vo35/vo35}$ was also used
570 (Erickson et al., 2019).

571 ***Genotyping***

572 To genotype *lhfpl5b*$^{vo35/vo35}$ larvae and siblings after mechanical stimulation and
573 immunohistochemical labeling, ~1 mm tail tissue was excised, and genomic DNA was extracted
574 by incubation in a lysis buffer (10 mM Tris pH 8.0, 50 mM KCl, 0.3% NP-40, 0.3% Tween-20). A
575 genomic region of *lhfpl5b* was amplified by PCR using forward primer
576 GCGTCATGTGGGCAGTTTTC and reverse primer TAGACACTAGCGGCGTTGC. The
577 *lhfpl5b*^{vo35} mutation disrupts a MluCI restriction site (AATT), so PCR products were digested with
578 MluCI, and homo- and heterozygotes were resolved by differences in band size on a 1-1.5%
579 agarose gel.

580 ***Experimental Apparatus***

581 Multi-well plates containing larvae were clamped to a custom magnesium head
582 expander (Vibration & Shock Technologies, Woburn, MA) on a vertically-oriented Brüel+Kjær
583 LDS Vibrator, V408 (Brüel and Kjær, Naerum, Denmark). An additional metal plate was fitted to
584 the bottom of the multi-well dish to fill a small gap between the bottoms of the wells and the

585 head expander to eliminate flexing of the well plate relative to the head expander. Vibrometry of
586 the well bottoms and the head expander with a laser-Dopper vibrometer (OFV-2600 and OFV-
587 501, Polytec, Irvine, CA) confirmed that the well plate and head expander motion were equal at
588 stimulus frequencies. This experimental apparatus was housed in a custom sound-attenuation
589 chamber. An Optiplex 3020 Mini Tower (Dell) with a NI PCIe-6321, X Series Multifunction DAQ
590 (National Instruments) running a custom stimulus generation program (modified version of
591 Cochlear Function Test Suite) was used to relay the stimulus signal to a Brüel+Kjær LDS
592 PA100E Amplifier that drove a controlled 60 Hz vibratory stimulus along the larvae's
593 dorsoventral axis (vertically). Two accelerometers (BU-21771, Knowles, Itasca, IL) were
594 mounted to the head expander to monitor the vertical displacement of the plate. The output of
595 the accelerometers was relayed through a custom accelerometer amplifier (EPL Engineering
596 Core). A block diagram for the EPL Lateral Line Stimulator can be found here:
597 https://www.masseyeandear.org/research/otolaryngology/eaton-peabody-
598 laboratories/engineering-core).

599 ***Mechanical overstimulation of lateral-line organs in free swimming larvae***

600 At 7 dpf, free-swimming zebrafish larvae were placed in untreated 6-well plates
601 (Corning, Cat# 3736; well diameter: 34.8 mm; total well volume: 16.8 ml) with 6 ml E3 per well,
602 pre-warmed to 29°C. Up to 15 larvae were placed in each well. Individual wells were sealed with
603 Glad® Press 'n Seal plastic food wrap prior to placing the lid on the plate. An additional metal
604 plate was fitted to the bottom of the multi-well dish to fill a small gap between the bottoms of the
605 wells and the head expander.

606 Mechanical water displacement exposures (stimulus parameters: 60 Hz, 40.3 ± 0.5 m/s^2)
607 were conducted at room temperature (22-24°C) up to 2 hours after dawn. The frequency
608 selected for mechanical overexposure of lateral-line organs was based on previous studies
609 showing 60 Hz to be within the optimal upper frequency range of mechanical sensitivity of
610 superficial posterior lateral-line neuromasts (Weeg and Bass 2002, Trapani et al, 2009, Levi et
611 al, 2015). To confirm that 60 Hz was the optimal frequency to induce damage, we tested 45, 60,
612 and 75 Hz at comparable intensities. We observed at 75 Hz no apparent damage to lateral line
613 neuromasts while 45 Hz at a comparable intensity proved toxic i.e. it was lethal to the fish.

614 Exposures consisted of 20 minutes of stimulation followed by a 10-minute break and 2
615 hours of uninterrupted stimulation. We also tested periodic exposures that consisted of a series
616 of short pulses spanning 2 hours total: 2 20-minute exposures each followed by 10 minutes of
617 rest, followed by 30 minutes of stimulation, a 10-minute break, and a final 20 minutes of
618 stimulation. During the entire duration of exposure, unexposed control fish were kept in the

619 same conditions as exposed fish i.e. placed in a multi-well dish and maintained in the same
620 room as the exposure chamber. For experiments pharmacologically blocking glutamate uptake,
621 fish were co-exposed to 10 μM DL-TBOA (Tocris; Cat. No.1223) + 0.1% DMSO or 0.1% DMSO
622 alone. After exposure, larvae were either immediately fixed for histology, prepared for live
623 imaging, or allowed to recover for up to 2 days in an incubator at 29°C.

624 ***Ablation of lateral-line organ with $CuSO_4$***

625 Free-swimming larvae were exposed to freshly made 3 μM $CuSO_4$ solution in E3 for 1
626 hour, then rinsed and allowed to recover for 2 hours to ensure complete ablation of the lateral-
627 line neuromasts. Neuromast ablation was confirmed by immunofluorescent labeling of hair cells.
628 The effects of low-dose copper exposure are likely specific to lateral-line organs; a previous
629 study in zebrafish determined exposure to low-dose $CuSO_4$ for 1 hour did not alter the acoustic
630 escape response, which is similar to the fast start response we observed but evoked by higher
631 frequency stimulation (100-500 Hz) of the anterior macula of inner ear (Buck, Winter, Redfern, &
632 Whitfield, 2012).

633 ***Fast-start escape response behavior assay***

634 Images of larval swimming behavior (1000 frames per second) were acquired with an
635 Edgertronic SC1 high-speed camera (Sanstreak Corp). Image acquisition began 10 seconds
636 following stimulus onset. All subsequent analysis was performed using ImageJ. To track
637 swimming behavior, images were initially stabilized using the Image Stabilizer Plugin. In
638 stabilized images, the position of individual larval heads (located via the pigmented eyes) in
639 each frame were tracked using the Manual Tracking Plugin. Larvae were tracked over 10
640 seconds (10,000 frames total) per trial. 'Fast start' responses—defined as a c-bend of the body
641 occurring within 15 ms followed by a counter-bend— were identified manually.

642 ***Whole-mount immunohistochemistry***

643 For visualization of zebrafish lateral-line hair cells, neurons, and synapses: 7-9 dpf
644 larvae were briefly sedated on ice, transferred to fixative (4% paraformaldehyde, 1% sucrose,
645 37.5 μM $CaCl_2$, 0.1 M phosphate buffer) in a flat-bottomed 2 ml Eppedorf tubes, and fixed for 5
646 hours at 4-8°C. Fixed larvae were permeabilized in ice-cold acetone for 5 minutes, then blocked
647 in phosphate-buffered saline (PBS) with 2% goat serum, 1% bovine serum albumin (BSA), and
648 1% DMSO for 2-4 hours at room temperature (RT; 22-24 °C). Larvae were incubated with
649 primary antibodies diluted in PBS with 1% BSA and 1% DMSO overnight at 4-8°C, followed by
650 several rinses in PBS/BSA/DMSO and incubation in diluted secondary antibodies conjugated to
651 Pacific Blue (1:400), Alexa Fluor 488 (1:1000), Alexa Fluor 555 (1:1000), Alexa Fluor 647
652 (1:1000; Invitrogen), or DyLight 549 (1:1000; Thermo-Fisher) for 2 hours at RT. In some

653 experiments, fixed larvae were stained with 2.5 ug/ml 4′,6-diamidino-2-phenylindole (DAPI;
654 Invitrogen) diluted in PBS to label all cell nuclei. Larvae were mounted on glass slides with
655 elvanol (13% w/v polyvinyl alcohol, 33% w/v glycerol, 1% w/v DABCO (1,4 diazobicylo[2,2,2]
656 octane) in 0.2 M Tris, pH 8.5) and #1.5 cover slips.
657 For visualization of inflammation and macrophage recruitment: 7 dpf larvae were
658 sedated on ice, transferred to 4% paraformaldehyde fixative in PBS, then fixed overnight at 4-
659 8°C. The next day larvae were rinsed in PBS and blocked in PBS with 5% normal horse serum
660 (NHS), 1% DMSO, and 1% Triton x-100 for 2 hours at RT. Larvae were incubated with primary
661 antibodies diluted in PBS with 5% NHS and 1% Triton-x 100 overnight at RT, rinsed several
662 times in PBS, then incubated in diluted secondary antibodies listed above for 2 hours at RT.
663 Larvae were mounted on glass slides with glycerol/PBS (9:1); coverslips were sealed with clear
664 nail polish.

665 ***Primary antibodies***

666 The following commercial antibodies were used in this study: GFP (1:500; Aves Labs,
667 Inc; Cat# GFP-1020), Parvalbumin (1:2000; Thermo Fisher; Cat# PA1-933), Parvalbumin
668 (1:2000; Abcam; Cat# ab11427), Parvalbumin (1:500; Sigma-Aldrich; Cat# P3088), MAGUK
669 (K28/86; 1:500; NeuroMab, UC Davis; Cat# 75-029), Otoferlin (1:500; Developmental Studies
670 Hybridoma Bank/ HCS-1). Custom affinity-purified antibody generated against *Danio rerio*
671 Ribeye b (mouse IgG2a; 1:2000; (Sheets et al., 2011)) was also used.

672 ***Hair-cell labeling***

673 To selectively label hair-cell nuclei, live zebrafish larvae were incubated with DAPI
674 diluted 1:2000 in E3 media for 4 minutes. Larvae were briefly rinsed 3 times in fresh E3 media,
675 then immediately exposed to mechanical overstimulation.
676 Live imaging of FM1-43 did not provide the temporal resolution needed to compare
677 relative uptake and fast recovery 0-4 hours following exposure. We therefore examined FM1-43
678 uptake using the fixable analogue. To label with FM1-43X (n-(3-triethylammoniumpropyl)-4-(4-
679 (dibutylamino)-styryl) pyridinium dibromide; ThermoFisher)), free-swimming larvae were
680 exposed to FM 1-43FX at 3 μM for 20 seconds, then rinsed 3 times in fresh E3 as previously
681 described (Toro et al., 2015) and immediately fixed (4% paraformaldehyde, 4% sucrose, 150
682 μM $CaCl_2$, 0.1 M phosphate buffer). FM 1-43FX mean signal intensity from maximum projection
683 images was calculated using ImageJ as the integrated pixel intensity divided by the area of the
684 neuromast region of interest. We verified that relative labeling of hair cells at 1-3 hours
685 appeared comparable between live FM1-43 and FM 1-43FX. We also verified loss of FM 1-

686 43FX uptake in larvae following brief treatment with 5 mM BAPTA to disrupt tip links (Kindt et
687 al., 2012). Following fixation, stereocilia were labeled by incubation with phalloidin conjugated to
688 Alexa Fluor 488 (Invitrogen) at 66 μM in PBS, washed, and mounted on slides with elvanol.

689 ***EdU labeling and quantification***

690 To label proliferating cells, we used the Click-iT EdU Cell Proliferation Kit for Imaging,
691 Alexa Fluor 555 dye (Invitrogen). Following mechanical overstimulation, larvae were incubated
692 in 500 μM EdU with 0.5% DMSO in E3 for 4 hours at 28°C then fixed in 4% paraformaldehyde
693 in PBS overnight at 4°C. Larvae were washed in 3% bovine serum albumin in PBS then
694 permeabilized with 0.5% Triton-X in PBS. GFP signal in Tg[tnks1bp1:GFP] fish was amplified
695 using anti-GFP primary antibody (Aves), followed by a secondary antibody conjugated to Alexa
696 Fluor 488. The EdU detection reaction was performed according to manufacturer guidelines;
697 larvae were incubated in a reaction cocktail (4 mM CuSO4 and Alexa Fluor 555 azide in 1X
698 Click-iT reaction buffer with reaction buffer additive) for 1 hour at 25°C. Larvae were washed,
699 counterstained with Hoechst 33342, and mounted on slides with elvanol. Confocal images of
700 neuromasts were acquired using an LSM 700 laser scanning confocal microscope with a 63x
701 1.4 NA Plan-Apochromat oil-immersion objective (Carl Zeiss). The numbers of EdU+ cells per
702 neuromast were quantified in ImageJ.

703 ***Confocal imaging***

704 Images of fixed samples were acquired using an LSM 700 laser scanning confocal
705 microscope with a 63x 1.4 NA Plan-Apochromat oil-immersion objective (Carl Zeiss). Confocal
706 stacks were collected with a z step of 0.3 μm over 7-10 μm with pixel size of 100 nm (x-y image
707 size 51 x 51 μm). Acquisition parameters were established using the brightest control specimen
708 such that just a few pixels reached saturation in order to achieve the greatest dynamic range in
709 our experiments. These parameters including gain, laser power, scan speed, dwell time,
710 resolution, and zoom, were kept consistent between comparisons.

711 ***Confocal image processing and analysis***

712 All analysis was performed on blinded images. Digital images were processed using
713 ImageJ software (Schneider, Rasband, & Eliceiri, 2012). In order to quantitatively measure sizes
714 and fluorescent intensities of puncta, raw images containing single immunolabel were
715 subtracted for background using a 20-pixel rolling ball radius and whole neuromasts were
716 delineated from Parvalbumin-labeled hair cells using the freehand selection and “synchronize
717 windows” tools. Puncta were defined as regions of immunolabel with pixel intensity above a
718 determined threshold: threshold for Ribeye label was calculated using the Isodata algorithm

719 (Ridler & Calvard, 1978) on maximum-intensity projections, threshold for MAGUK label was
720 calculated as the product of 7 times the average pixel intensity of the whole neuromast region in
721 a maximum-intensity projection. Particle volume and intensity were measured using the 3D
722 object counter (Bolte & Cordelieres, 2006) using a lower threshold and a minimum size of 10
723 voxels. To normalize for differences in staining intensity across experimental trials, all volumes
724 were divided by the median control volume in each trial for each individual channel. The number
725 of particles above lower threshold was quantified using the ImageJ Maximum Finder plugin with
726 a noise tolerance of 10 on maximum-intensity projections. Intact synapses were manually
727 counted and defined as adjoining or overlapping maxima of Ribeye and MAGUK labels. The
728 number of synapses per hair cell was approximated by dividing the number of intact synapses
729 within an neuromast by the number of hair cells in the neuromast. Innervation of neuromast hair
730 cells was quantified during blinded analysis by scrolling through confocal z-stacks of each
731 neuromast (step size 0.3 μm) containing hair cell and afferent labeling and identifying hair cells
732 that were not directly contacted by an afferent neuron i.e. no discernable space between the
733 hair cell and the neurite. Hair cells that were identified as no longer innervated showed
734 measurable neurite retraction; there was generally >0.5 μm distance between a retracted
735 neurite and hair cell. Stereocilia length measurements were obtained in ImageJ from
736 interpolated 3D projections of z-stack images (step size 0.3 μm) containing phalloidin labeled
737 hair bundles. Three independent measurements were obtained from the base to the tips of hair
738 bundles at center of each neuromast, and the average length was calculated.
739 Quantitative data on macrophage response to mechanical injury were collected from the
740 two caudal-most ('terminal') neuromasts. Confocal image stacks were obtained using a Zeiss
741 LSM700 microscope and visualized using Volocity software. These image stacks were used to
742 derive three metrics from each neuromast. First, the number of macrophages within 25 μm of a
743 particular neuromast was determined by inscribing a circle of 25 μm radius, centered on the
744 neuromast, and counting the number of macrophages that were either fully or partially enclosed
745 by this circle. Next, the number of macrophages contacting a neuromast was determined by
746 scrolling through the x-y planes of each image stack (1 μm interval between x-y planes, 15 μm
747 total depth) and the counting macrophages that were in direct contact with Otoferlin-labeled hair
748 cells. Finally, the number of macrophages that had internalized Otoferlin-labeled material (hair-
749 cell debris) were counted and were assumed to reflect the number of phagocytic events. For
750 each metric, the recorded number reflected the activity of a single macrophage, i.e., a
751 macrophage that made contacts with multiple hair cells and/or had internalized debris from
752 several hair cells was still classified as a single 'event.'

753 Subsequent image processing for display within figures was performed using Photoshop
754 and Illustrator software (Adobe).

755 ***Scanning electron microscopy***

756 To image hair-cell bundles, zebrafish larvae were exposed to strong water wave
757 stimulus, then anesthetized in 0.12% tricaine in E3 and immediately fixed in 2.5%
758 glutaraldehyde in 0.1 M sodium cacodylate buffer (Electron Microscopy Sciences)
759 supplemented with 2 mM $CaCl_2$. Larvae were shipped overnight in fixative, then most of the
760 fixative (~90-95%) was removed, replaced with distilled water, and samples were stored at 4C.
761 Next, larvae were washed in distilled water (Gibco), dehydrated with an ascending series of
762 ethanol, critical point dried from liquid CO_2 (Tousimis Aurosamdri 815), mounted on adhesive
763 carbon tabs (TedPella), sputter coated with 5 nm of platinum (Leica EM ACE600), and imaged
764 on Hitachi S-4700 scanning electron microscope. Kinocilia diameter measurements were
765 performed using ImageJ.

766 ***Statistical analysis***

767 A hierarchical linear model analysis with fish used as random effects was used to
768 compare each of the measures between the conditions and groups. Akaike Information Criterion
769 (AIC) and Bayessian Information Criterion (BIC) were used to identify the best fitted covariance
770 structure. Tukey's adjustment was used for the alpha level to avoid type I error inflation due to
771 multiple comparisons. Estimated marginal mean differences and 95% Confidence Intervals
772 around them were explored and reported for quantification of effect size for group differences.
773 Graphs for data visualization and additional statistical analyses were performed Prism 8
774 (Graphpad Software Inc). Mixed model analysis was used to compare time-series data.
775 Statistical significance between synaptic ribbon and PSD volumes with was determined by
776 Kruskal-Wallis test (one independent variable) or Mann–Whitney U test (one independent
777 variable) and appropriate post-hoc tests. Based on the variance and effect sizes reported in
778 previous studies, the number of biological replicates were suitable to provide statistical power to
779 avoid Type II error (Sebe et al., 2017; Uribe et al., 2018).
780

781

782 References

783 Behra, M., Gallardo, V. E., Bradsher, J., Torrado, A., Elkahloun, A., Idol, J., . . . Burgess, S. M.
784 (2012). Transcriptional signature of accessory cells in the lateral line, using the
785 Tnk1bp1:EGFP transgenic zebrafish line. *BMC Dev Biol, 12*, 6. doi:10.1186/1471-213X-
786 12-6
787 Bhandiwad, A. A., Zeddies, D. G., Raible, D. W., Rubel, E. W., & Sisneros, J. A. (2013).
788 Auditory sensitivity of larval zebrafish (Danio rerio) measured using a behavioral
789 prepulse inhibition assay. *The Journal of experimental biology, 216*(Pt 18), 3504-3513.
790 doi:10.1242/jeb.087635
791 Bolte, S., & Cordelieres, F. P. (2006). A guided tour into subcellular colocalization analysis in
792 light microscopy. *J Microsc, 224*(Pt 3), 213-232. doi:10.1111/j.1365-2818.2006.01706.x
793 Buck, L. M., Winter, M. J., Redfern, W. S., & Whitfield, T. T. (2012). Ototoxin-induced cellular
794 damage in neuromasts disrupts lateral line function in larval zebrafish. *Hear Res, 284*(1-
795 2), 67-81. doi:10.1016/j.heares.2011.12.001
796 Bullen, A., Anderson, L., Bakay, W., & Forge, A. (2019). Localized disorganization of the
797 cochlear inner hair cell synaptic region after noise exposure. *Biol Open, 8*(1).
798 doi:10.1242/bio.038547
799 Burgess, H. A., & Granato, M. (2007). Sensorimotor gating in larval zebrafish. *The Journal of*
800 *neuroscience : the official journal of the Society for Neuroscience, 27*(18), 4984-4994.
801 doi:10.1523/JNEUROSCI.0615-07.2007
802 Carpaneto Freixas, A. E., Moglie, M. J., Castagnola, T., Salatino, L., Domene, S., Marcovich, I.,
803 . . . Elgoyhen, A. B. (2021). Unraveling the Molecular Players at the Cholinergic Efferent
804 Synapse of the Zebrafish Lateral Line. *J Neurosci, 41*(1), 47-60.
805 doi:10.1523/JNEUROSCI.1772-20.2020
806 Carrillo, S. A., Anguita-Salinas, C., Pena, O. A., Morales, R. A., Munoz-Sanchez, S., Munoz-
807 Montecinos, C., . . . Allende, M. L. (2016). Macrophage Recruitment Contributes to
808 Regeneration of Mechanosensory Hair Cells in the Zebrafish Lateral Line. *J Cell*
809 *Biochem, 117*(8), 1880-1889. doi:10.1002/jcb.25487
810 Chen, Z., Kujawa, S. G., & Sewell, W. F. (2010). Functional roles of high-affinity glutamate
811 transporters in cochlear afferent synaptic transmission in the mouse. *J Neurophysiol,*
812 *103*(5), 2581-2586. doi:10.1152/jn.00018.2010
813 Cho, S. I., Gao, S. S., Xia, A., Wang, R., Salles, F. T., Raphael, P. D., . . . Oghalai, J. S. (2013).
814 Mechanisms of hearing loss after blast injury to the ear. *PLoS One, 8*(7), e67618.
815 doi:10.1371/journal.pone.0067618
816 Coffin, A. B., Kelley, M. W., Manley, G. A., & Popper, A. N. (2004). Evolution of sensory hair
817 cells. In G. A. Manley, R. R. Fay, & A. N. Popper (Eds.), *Evolution of the Auditory*
818 *System*. New York: Springer-Verlag.
819 Cruz, I. A., Kappedal, R., Mackenzie, S. M., Hailey, D. W., Hoffman, T. L., Schilling, T. F., &
820 Raible, D. W. (2015). Robust regeneration of adult zebrafish lateral line hair cells reflects
821 continued precursor pool maintenance. *Dev Biol, 402*(2), 229-238.
822 doi:10.1016/j.ydbio.2015.03.019
823 Davies, C., Tingley, D., Kachar, B., Wenthold, R. J., & Petralia, R. S. (2001). Distribution of
824 members of the PSD-95 family of MAGUK proteins at the synaptic region of inner and
825 outer hair cells of the guinea pig cochlea. *Synapse, 40*(4), 258-268.
826 doi:10.1002/syn.1048
827 Dow, E., Jacobo, A., Hossain, S., Siletti, K., & Hudspeth, A. J. (2018). Connectomics of the
828 zebrafish's lateral-line neuromast reveals wiring and miswiring in a simple microcircuit.
829 *Elife, 7*. doi:10.7554/eLife.33988

830 Erickson, T., Pacentine, I. V., Venuto, A., Clemens, R., & Nicolson, T. (2019). The lhfpl5
831 Ohnologs lhfpl5a and lhfpl5b Are Required for Mechanotransduction in Distinct
832 Populations of Sensory Hair Cells in Zebrafish. *Front Mol Neurosci, 12*, 320.
833 doi:10.3389/fnmol.2019.00320
834 Faucherre, A., Pujol-Marti, J., Kawakami, K., & Lopez-Schier, H. (2009). Afferent neurons of the
835 zebrafish lateral line are strict selectors of hair-cell orientation. *PloS one, 4*(2), e4477.
836 doi:10.1371/journal.pone.0004477
837 Fernandez, K. A., Guo, D., Micucci, S., De Gruttola, V., Liberman, M. C., & Kujawa, S. G.
838 (2020). Noise-induced Cochlear Synaptopathy with and Without Sensory Cell Loss.
839 *Neuroscience, 427*, 43-57. doi:10.1016/j.neuroscience.2019.11.051
840 Gao, W. Y., Ding, D. L., Zheng, X. Y., Ruan, F. M., & Liu, Y. J. (1992). A comparison of changes
841 in the stereocilia between temporary and permanent hearing losses in acoustic trauma.
842 *Hearing research, 62*(1), 27-41. Retrieved from
843 http://www.ncbi.nlm.nih.gov/pubmed/1429249
844 Glowatzki, E., & Fuchs, P. A. (2002). Transmitter release at the hair cell ribbon synapse. *Nature*
845 *neuroscience, 5*(2), 147-154. doi:10.1038/nn796
846 Henry, W. R., & Mulroy, M. J. (1995). Afferent synaptic changes in auditory hair cells during
847 noise-induced temporary threshold shift. *Hearing research, 84*(1-2), 81-90. Retrieved
848 from http://www.ncbi.nlm.nih.gov/pubmed/7642458
849 Hickman, T. T., Smalt, C., Bobrow, J., Quatieri, T., & Liberman, M. C. (2018). Blast-induced
850 cochlear synaptopathy in chinchillas. *Sci Rep, 8*(1), 10740. doi:10.1038/s41598-018-
851 28924-7
852 Hirose, K., Discolo, C. M., Keasler, J. R., & Ransohoff, R. (2005). Mononuclear phagocytes
853 migrate into the murine cochlea after acoustic trauma. *The Journal of comparative*
854 *neurology, 489*(2), 180-194. doi:10.1002/cne.20619
855 Hirose, K., Rutherford, M. A., & Warchol, M. E. (2017). Two cell populations participate in
856 clearance of damaged hair cells from the sensory epithelia of the inner ear. *Hear Res,*
857 *352*, 70-81. doi:10.1016/j.heares.2017.04.006
858 Holmgren, M., & Sheets, L. (2021). Influence of Mpv17 on Hair-Cell Mitochondrial Homeostasis,
859 Synapse Integrity, and Vulnerability to Damage in the Zebrafish Lateral Line. *Front Cell*
860 *Neurosci, 15*, 693375. doi:10.3389/fncel.2021.693375
861 Hu, N., Rutherford, M. A., & Green, S. H. (2020). Protection of cochlear synapses from noise-
862 induced excitotoxic trauma by blockade of Ca(2+)-permeable AMPA receptors. *Proc Natl*
863 *Acad Sci U S A, 117*(7), 3828-3838. doi:10.1073/pnas.1914247117
864 Husbands, J. M., Steinberg, S. A., Kurian, R., & Saunders, J. C. (1999). Tip-link integrity on
865 chick tall hair cell stereocilia following intense sound exposure. *Hear Res, 135*(1-2), 135-
866 145. doi:10.1016/s0378-5955(99)00101-x
867 Indzhykulian, A. A., Stepanyan, R., Nelina, A., Spinelli, K. J., Ahmed, Z. M., Belyantseva, I. A., .
868 . . Frolenkov, G. I. (2013). Molecular remodeling of tip links underlies mechanosensory
869 regeneration in auditory hair cells. *PLoS Biol, 11*(6), e1001583.
870 doi:10.1371/journal.pbio.1001583
871 Jia, S., Yang, S., Guo, W., & He, D. Z. (2009). Fate of mammalian cochlear hair cells and
872 stereocilia after loss of the stereocilia. *J Neurosci, 29*(48), 15277-15285.
873 doi:10.1523/JNEUROSCI.3231-09.2009
874 Kaur, T., Clayman, A. C., Nash, A. J., Schrader, A. D., Warchol, M. E., & Ohlemiller, K. K.
875 (2019). Lack of Fractalkine Receptor on Macrophages Impairs Spontaneous Recovery of
876 Ribbon Synapses After Moderate Noise Trauma in C57BL/6 Mice. *Front Neurosci, 13*,
877 620. doi:10.3389/fnins.2019.00620
878 Kaur, T., Zamani, D., Tong, L., Rubel, E. W., Ohlemiller, K. K., Hirose, K., & Warchol, M. E.
879 (2015). Fractalkine Signaling Regulates Macrophage Recruitment into the Cochlea and

Promotes the Survival of Spiral Ganglion Neurons after Selective Hair Cell Lesion. *J Neurosci, 35*(45), 15050-15061. doi:10.1523/JNEUROSCI.2325-15.2015

Kim, K. X., Payne, S., Yang-Hood, A., Li, S. Z., Davis, B., Carlquist, J., . . . Rutherford, M. A. (2019). Vesicular Glutamatergic Transmission in Noise-Induced Loss and Repair of Cochlear Ribbon Synapses. *The Journal of neuroscience : the official journal of the Society for Neuroscience, 39*(23), 4434-4447. doi:10.1523/JNEUROSCI.2228-18.2019

Kindt, K. S., Finch, G., & Nicolson, T. (2012). Kinocilia mediate mechanosensitivity in developing zebrafish hair cells. *Developmental cell, 23*(2), 329-341. doi:10.1016/j.devcel.2012.05.022

Kindt, K. S., & Sheets, L. (2018). Transmission Disrupted: Modeling Auditory Synaptopathy in Zebrafish. *Front Cell Dev Biol, 6*, 114. doi:10.3389/fcell.2018.00114

Kniss, J. S., Jiang, L., & Piotrowski, T. (2016). Insights into sensory hair cell regeneration from the zebrafish lateral line. *Curr Opin Genet Dev, 40*, 32-40. doi:10.1016/j.gde.2016.05.012

Kujawa, S. G., & Liberman, M. C. (2009). Adding insult to injury: cochlear nerve degeneration after "temporary" noise-induced hearing loss. *The Journal of neuroscience : the official journal of the Society for Neuroscience, 29*(45), 14077-14085. doi:10.1523/JNEUROSCI.2845-09.2009

LeMasurier, M., & Gillespie, P. G. (2005). Hair-cell mechanotransduction and cochlear amplification. *Neuron, 48*(3), 403-415. doi:10.1016/j.neuron.2005.10.017

Levi, R., Akanyeti, O., Ballo, A., & Liao, J. C. (2015). Frequency response properties of primary afferent neurons in the posterior lateral line system of larval zebrafish. *J Neurophysiol, 113*(2), 657-668. doi:10.1152/jn.00414.2014

McHenry, M. J., Feitl, K. E., Strother, J. A., & Van Trump, W. J. (2009). Larval zebrafish rapidly sense the water flow of a predator's strike. *Biol Lett, 5*(4), 477-479. doi:10.1098/rsbl.2009.0048

Merchan-Perez, A., & Liberman, M. C. (1996). Ultrastructural differences among afferent synapses on cochlear hair cells: correlations with spontaneous discharge rate. *J Comp Neurol, 371*(2), 208-221. doi:10.1002/(SICI)1096-9861(19960722)371:2<208::AID-CNE2>3.0.CO;2-6

Nair, A., Azatian, G., & McHenry, M. J. (2015). The kinematics of directional control in the fast start of zebrafish larvae. *J Exp Biol, 218*(Pt 24), 3996-4004. doi:10.1242/jeb.126292

Nordmann, A. S., Bohne, B. A., & Harding, G. W. (2000). Histopathological differences between temporary and permanent threshold shift. *Hearing research, 139*(1-2), 13-30. Retrieved from http://www.ncbi.nlm.nih.gov/pubmed/10601709

Nüsslein-Volhard, C., & Dahm, R. (2002). *Zebrafish : a practical approach* (1st ed.). Oxford: Oxford University Press.

Obholzer, N., Wolfson, S., Trapani, J. G., Mo, W., Nechiporuk, A., Busch-Nentwich, E., . . . Nicolson, T. (2008). Vesicular glutamate transporter 3 is required for synaptic transmission in zebrafish hair cells. *The Journal of neuroscience : the official journal of the Society for Neuroscience, 28*(9), 2110-2118. doi:10.1523/JNEUROSCI.5230-07.2008

Olivari, F. A., Hernandez, P. P., & Allende, M. L. (2008). Acute copper exposure induces oxidative stress and cell death in lateral line hair cells of zebrafish larvae. *Brain Res, 1244*, 1-12. doi:10.1016/j.brainres.2008.09.050

Puel, J. L., Ruel, J., Gervais d'Aldin, C., & Pujol, R. (1998). Excitotoxicity and repair of cochlear synapses after noise-trauma induced hearing loss. *Neuroreport, 9*(9), 2109-2114. Retrieved from http://www.ncbi.nlm.nih.gov/pubmed/9674603

Qiu, X., & Muller, U. (2018). Mechanically Gated Ion Channels in Mammalian Hair Cells. *Front Cell Neurosci, 12*, 100. doi:10.3389/fncel.2018.00100

Ridler, T. W., & Calvard, S. (1978). Picture Thresholding Using an Iterative Selection Method. *3EEE TRANSACTIONS ON SYSTEMS, MAN, AND CYBERNETICS*(8), 630 - 632. doi:https://doi.org/10.1109/TSMC.1978.4310039

Roca, F. J., & Ramakrishnan, L. (2013). TNF dually mediates resistance and susceptibility to mycobacteria via mitochondrial reactive oxygen species. *Cell, 153*(3), 521-534. doi:10.1016/j.cell.2013.03.022

Schneider, C. A., Rasband, W. S., & Eliceiri, K. W. (2012). NIH Image to ImageJ: 25 years of image analysis. *Nat Methods, 9*(7), 671-675. doi:10.1038/nmeth.2089

Sebe, J. Y., Cho, S., Sheets, L., Rutherford, M. A., von Gersdorff, H., & Raible, D. W. (2017). Ca(2+)-Permeable AMPARs Mediate Glutamatergic Transmission and Excitotoxic Damage at the Hair Cell Ribbon Synapse. *J Neurosci, 37*(25), 6162-6175. doi:10.1523/JNEUROSCI.3644-16.2017

Sheets, L., Kindt, K. S., & Nicolson, T. (2012). Presynaptic CaV1.3 channels regulate synaptic ribbon size and are required for synaptic maintenance in sensory hair cells. *The Journal of neuroscience : the official journal of the Society for Neuroscience, 32*(48), 17273-17286. doi:10.1523/JNEUROSCI.3005-12.2012

Sheets, L., Trapani, J. G., Mo, W., Obholzer, N., & Nicolson, T. (2011). Ribeye is required for presynaptic Ca(V)1.3a channel localization and afferent innervation of sensory hair cells. *Development, 138*(7), 1309-1319. doi:10.1242/dev.059451

Shi, L., Liu, L., He, T., Guo, X., Yu, Z., Yin, S., & Wang, J. (2013). Ribbon synapse plasticity in the cochleae of Guinea pigs after noise-induced silent damage. *PloS one, 8*(12), e81566. doi:10.1371/journal.pone.0081566

Slepecky, N. (1986). Overview of mechanical damage to the inner ear: noise as a tool to probe cochlear function. *Hear Res, 22*, 307-321. doi:10.1016/0378-5955(86)90107-3

Song, Q., Shen, P., Li, X., Shi, L., Liu, L., Wang, J., . . . Yin, S. (2016). Coding deficits in hidden hearing loss induced by noise: the nature and impacts. *Scientific reports, 6*, 25200. doi:10.1038/srep25200

Thomas, A. J., Wu, P., Raible, D. W., Rubel, E. W., Simon, J. A., & Ou, H. C. (2015). Identification of small molecule inhibitors of cisplatin-induced hair cell death: results of a 10,000 compound screen in the zebrafish lateral line. *Otology & neurotology : official publication of the American Otological Society, American Neurotology Society [and] European Academy of Otology and Neurotology, 36*(3), 519-525. doi:10.1097/MAO.0000000000000487

Toro, C., Trapani, J. G., Pacentine, I., Maeda, R., Sheets, L., Mo, W., & Nicolson, T. (2015). Dopamine Modulates the Activity of Sensory Hair Cells. *The Journal of neuroscience : the official journal of the Society for Neuroscience, 35*(50), 16494-16503. doi:10.1523/JNEUROSCI.1691-15.2015

Trapani, J. G., & Nicolson, T. (2010). Physiological recordings from zebrafish lateral-line hair cells and afferent neurons. *Methods in cell biology, 100*, 219-231. doi:10.1016/B978-0-12-384892-5.00008-6

Uribe, P. M., Villapando, B. K., Lawton, K. J., Fang, Z., Gritsenko, D., Bhandiwad, A., . . . Coffin, A. B. (2018). Larval Zebrafish Lateral Line as a Model for Acoustic Trauma. *eNeuro, 5*(4). doi:10.1523/ENEURO.0206-18.2018

Wagner, E. L., & Shin, J. B. (2019). Mechanisms of Hair Cell Damage and Repair. *Trends Neurosci, 42*(6), 414-424. doi:10.1016/j.tins.2019.03.006

Wan, G., Gomez-Casati, M. E., Gigliello, A. R., Liberman, M. C., & Corfas, G. (2014). Neurotrophin-3 regulates ribbon synapse density in the cochlea and induces synapse regeneration after acoustic trauma. *eLife, 3*. doi:10.7554/eLife.03564

Wang, H., Yin, S., Yu, Z., Huang, Y., & Wang, J. (2011). Dynamic changes in hair cell stereocilia and cochlear transduction after noise exposure. *Biochem Biophys Res Commun, 409*(4), 616-621. doi:10.1016/j.bbrc.2011.05.049

Wang, X., Zhu, Y., Long, H., Pan, S., Xiong, H., Fang, Q., . . . Sha, S. H. (2018). Mitochondrial Calcium Transporters Mediate Sensitivity to Noise-Induced Losses of Hair Cells and Cochlear Synapses. *Front Mol Neurosci, 11*, 469. doi:10.3389/fnmol.2018.00469

Warchol, M. E. (2011). Sensory regeneration in the vertebrate inner ear: differences at the levels of cells and species. *Hear Res, 273*(1-2), 72-79. doi:10.1016/j.heares.2010.05.004

Warchol, M. E. (2019). Interactions between Macrophages and the Sensory Cells of the Inner Ear. *Cold Spring Harb Perspect Med, 9*(6). doi:10.1101/cshperspect.a033555

Warchol, M. E., Schrader, A., & Sheets, L. (2021). Macrophages Respond Rapidly to Ototoxic Injury of Lateral Line Hair Cells but Are Not Required for Hair Cell Regeneration. *Front Cell Neurosci, 14*, 613246. doi:10.3389/fncel.2020.613246

Weeg, M. S., Fay, R. R., & Bass, A. H. (2002). Directionality and frequency tuning of primary saccular afferents of a vocal fish, the plainfin midshipman (Porichthys notatus). *J Comp Physiol A Neuroethol Sens Neural Behav Physiol, 188*(8), 631-641. doi:10.1007/s00359-002-0338-2

Williams, J. A., & Holder, N. (2000). Cell turnover in neuromasts of zebrafish larvae. *Hear Res, 143*(1-2), 171-181. doi:10.1016/s0378-5955(00)00039-3

Wong, H. C., Zhang, Q., Beirl, A. J., Petralia, R. S., Wang, Y. X., & Kindt, K. (2019). Synaptic mitochondria regulate hair-cell synapse size and function. *Elife, 8*. doi:10.7554/eLife.48914

Wynn, T. A., & Vannella, K. M. (2016). Macrophages in Tissue Repair, Regeneration, and Fibrosis. *Immunity, 44*(3), 450-462. doi:10.1016/j.immuni.2016.02.015

Xiao, Y., Faucherre, A., Pola-Morell, L., Heddleston, J. M., Liu, T. L., Chew, T. L., . . . Lopez-Schier, H. (2015). High-resolution live imaging reveals axon-glia interactions during peripheral nerve injury and repair in zebrafish. *Dis Model Mech, 8*(6), 553-564. doi:10.1242/dmm.018184

Zhang, Q., Li, S., Wong, H. C., He, X. J., Beirl, A., Petralia, R. S., . . . Kindt, K. S. (2018). Synaptically silent sensory hair cells in zebrafish are recruited after damage. *Nat Commun, 9*(1), 1388. doi:10.1038/s41467-018-03806-8

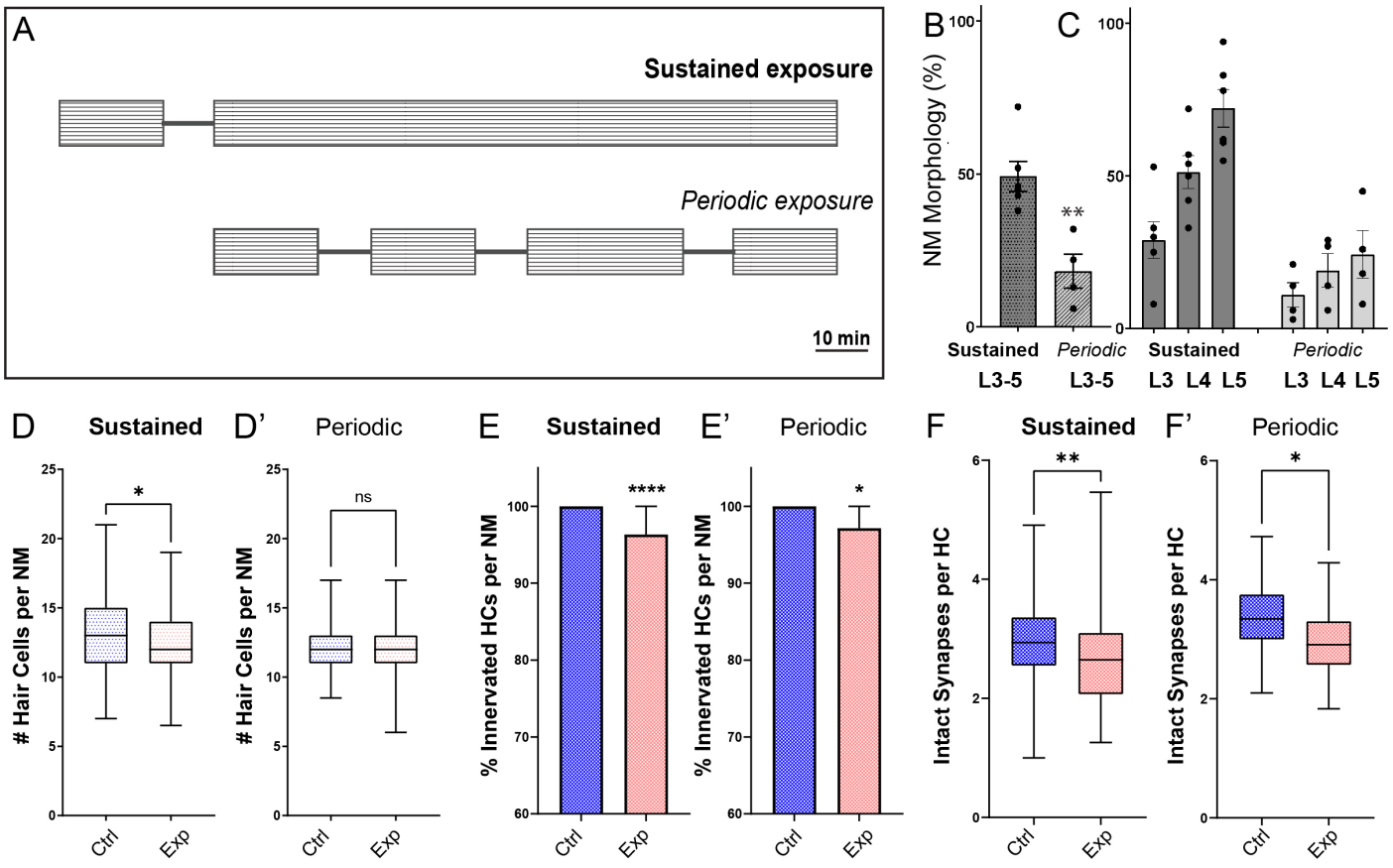

Supplemental Figure 1: Fish exposed to periodic stimulus have less mechanical damage to* neuromasts*, but still show synapse loss. **(A)** Schematic of the two exposure protocols. Sustained exposure was a 20 min. pulse followed by 120 minutes uninterrupted mechanical overstimulation; periodic exposure was 90 min. exposure with intermittent 10 min. breaks totaling 120 minutes. **(B)** Periodic stimulus causes less neuromast disruption. Immediately following sustained exposure, 46% of exposed neuromasts showed a "disrupted" phenotype, whereas following a periodic exposure only 17% of the neuromasts appeared "disrupted" (Unpaired t-test **P=0.0034). **(C)** Position of the neuromast along the tail was also associated with vulnerability to disruption with both sustained and periodic stimulation. **(D-F')** Measurements of hair-cell number, innervation, and synapse number averaged from individual fish (neuromasts L3-L5). **(D-D')** Average hair cell number per neuromast following exposure. With periodic exposure, the number of hair cells was comparable to control (*P=0.108 sustained, P=0.7233 periodic). **(E-E')** % of neuromast hair cells innervated (****P<0.0001 sustained, P=0.0156 periodic). **(F-F')** Average number of intact synapses per neuromast. There is significant loss of synapses with both periodic and sustained exposures (**P=0.0045 sustained, *P=0.0236 periodic).

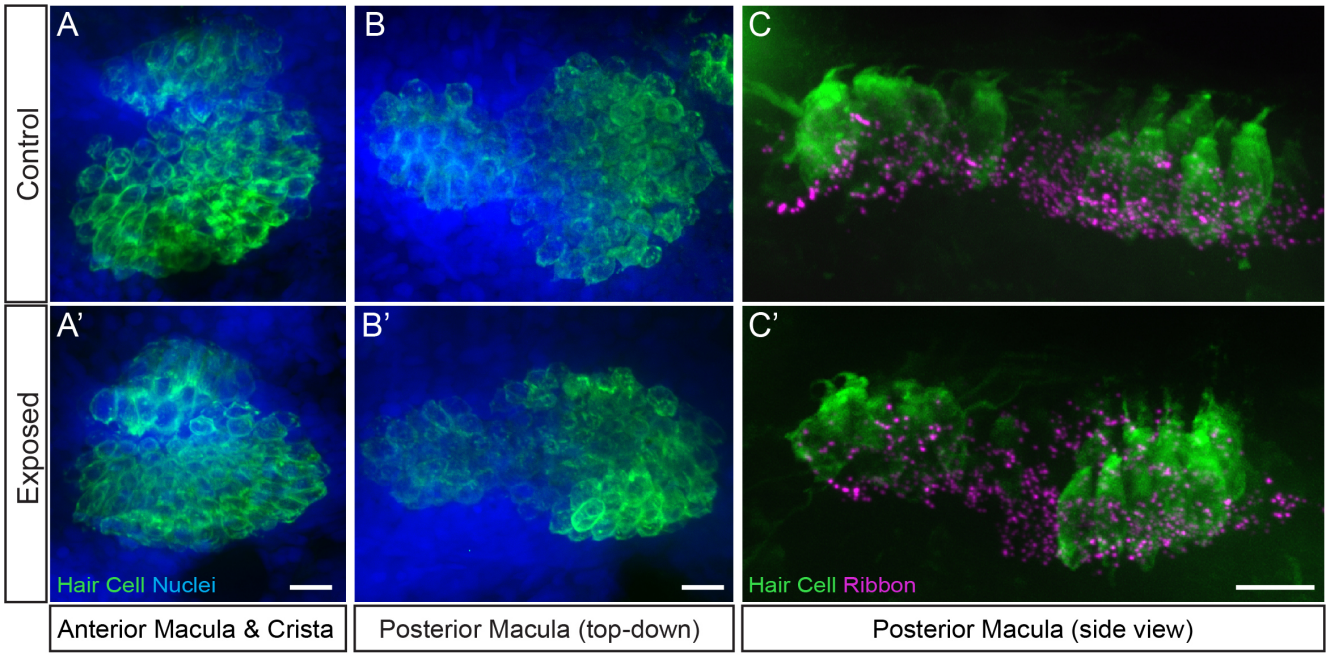

Supplemental Figure 2: Hair cell organs of the ear appeared undamaged in larvae exposed to sustained stimulus. Representative maximum intensity images of hair cell organs in the ears of control **(A-C)** and larvae exposed to sustained strong water wave stimulus **(A'-C')**. Hair cells in A-B were immunolabeled with an antibody against Otoferlin; posterior macula in C were immunolabled with antibodies against Parvalbumin to label hair cells and CtBP to label synaptic ribbons. Scale bars: 10 µm

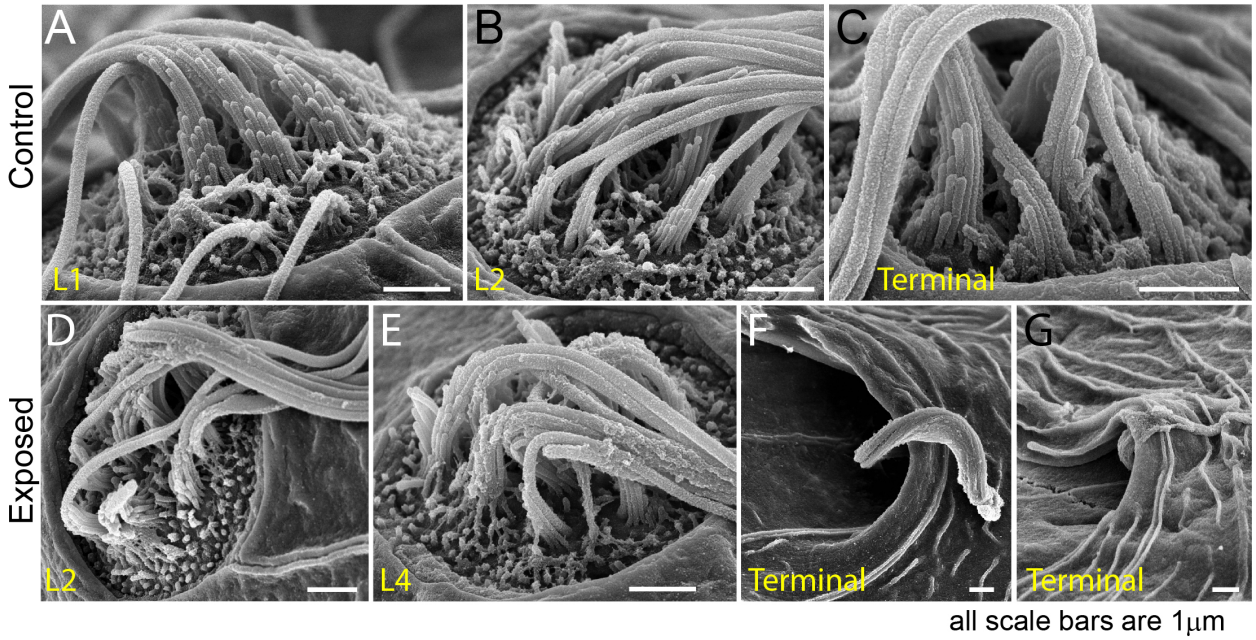

Supplemental Figure 3: Scanning electron microscopy imaging of tail neuromasts following mechanical injury confirms the damage is more prominent for posterior neuromasts. **(A-C)** Representative images of tail neuromasts of control fish larvae, presented as they are positioned on the larva: L1, L2 and terminal neuromasts. Each hair cell carries a tubulin-based primary cilium (kinocilium), which is thicker than the multiple mechanosensitive stereocilia arranged in a staircase. **(D-G)** Examples of tail neuromasts immediately following sustained stimulus exposure, presented as they are positioned on the larva: L2, L4, and two terminal neuromasts highlighting different levels of damage, with much more pronounced damage evident on terminal neuromasts. Scale bars: 1 μm

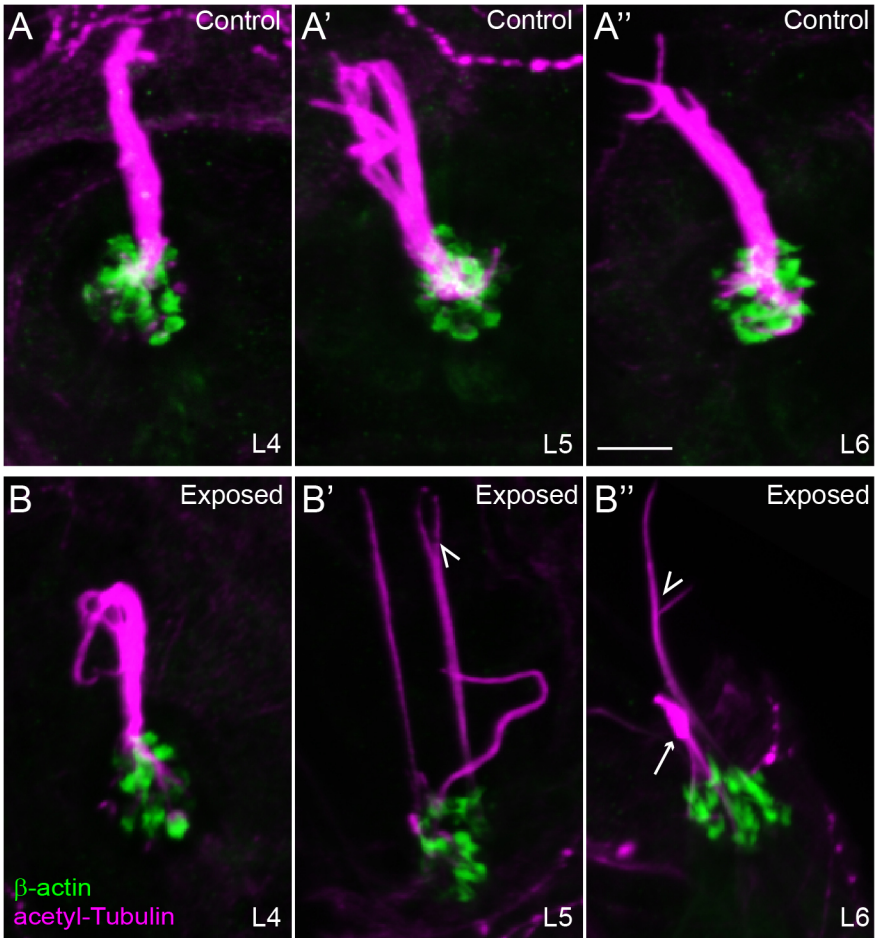

Supplemental Figure 4: Confocal images show damaged kinocilia following mechanical injury.
Representative confocal images of hair cell kinocilia (acetylated tubulin immunolabel; magenta) and stereocilia (βactin-GFP; green) in control (A-A'') and exposed (B-B'') larval neuromast L4-6 immediately following sustained strong water wave stimulus. Kinocilia appear as intact bundles in the control neuromasts. Arrow indicated kinocilial swelling, arrowheads indicate split kinocilia in the exposed neuromasts. Scale bar: 5 µm

Supplemental Movies
Swimming behavior of 7-day-old larvae during exposure to the strong water wave stimulus shown in Figure 2 over 500ms (1000 fps/ 500 frames).

Movie S1: Swimming behavior of control fish with intact lateral line organs. Magenta circle indicates a fish prior to a"fast escape" response.

Movie S2: Swimming behavior of larvae whose lateral-line neuromasts were ablated with $CuSO_4$. Magenta circles indicate larvae that were swept into the waves and could no longer tracked.